Kurisu Shusaku (Orcid ID: 0000-0002-4876-4419)

Proximal deposition of collagen IV by fibroblasts contributes to basement membrane formation by colon epithelial cells *in vitro*

Aya Tentaku[1,2], Shusaku Kurisu[1,5], Kurumi Sejima[1,4], Toshiki Nagao[1,4], Akira Takahashi[2], and Shigenobu Yonemura[1,3,5]

[1]Department of Cell Biology, Tokushima University Graduate School of Biomedical Sciences, Tokushima, Japan.

[2]Department of Preventive Environment and Nutrition, Tokushima University Graduate School of Biomedical Sciences, Tokushima, Japan.

[3]Laboratory for Ultrastructural Research, RIKEN Center for Biosystems Dynamics Research, Kobe, Japan.

[4]Student Lab, Tokushima University Graduate School of Biomedical Sciences, Tokushima, Japan.

[5]Corresponding authors:

Email: kurisu@tokushima-u.ac.jp

Tel.: +81-88-633-9258

or,

Email: yonemura.shigenobu@tokushima-u.ac.jp

Tel.: +81-88-633-7055

Tokushima University Graduate School of Biomedical Sciences,
Kuramoto-cho 3-18-15, Tokushima-shi, Tokushima 770-8503, Japan.

Running title:

BM collagen IV deposition by proximal fibroblasts

Conflicts of interest:

The authors declare no conflict of interest associated with this manuscript.

Keywords:

Basement membrane; collagen IV; fibroblast; colon epithelium; co-culture

This article has been accepted for publication and undergone full peer review but has not been through the copyediting, typesetting, pagination and proofreading process which may lead to differences between this version and the Version of Record. Please cite this article as doi: 10.1111/febs.16559

Abstract

The basement membrane (BM) underlying epithelial tissue is a thin layer of extracellular matrix that governs tissue integrity and function. Epithelial BMs are generally assembled using BM components secreted from two origins: epithelium and stroma. Although *de novo* BM formation involves self-assembly processes of large proteins, it remains unclear how stroma-derived macromolecules are transported and assembled, specifically in the BM region. In this study, we established an *in vitro* co-culture model of BM formation in which DLD-1 human colon epithelial cells were cultured on top of collagen I gel containing human embryonic OUMS-36T-2 fibroblasts as stromal cells. A distinct feature of our system is represented by OUMS-36T-2 cells which are almost exclusively responsible for synthesis of collagen IV, a major BM component. Exploiting this advantage, we found that collagen IV incorporation was significantly impaired in culture conditions where OUMS-36T-2 cells were not allowed to directly contact DLD-1 cells. Soluble collagen IV, once diluted in the culture medium, did not accumulate in the BM region efficiently. Live imaging of fluorescently tagged collagen IV revealed that OUMS-36T-2 cells deposited collagen IV aggregates directly onto the basal surface of DLD-1 cells. Collectively, these results indicate a novel mode of collagen IV deposition in which fibroblasts proximal to epithelial cells exclusively contribute to collagen IV assembly during BM formation.

Abbreviations

36T-2
: OUMS-36T-2

AA2P
: L-ascorbic acid 2-phosphate sesquimagnesium salt hydrate

AF
: Alexa Fluor

BM
: basement membrane

CBB
: Coomassie brilliant blue

EGFP
: enhanced green fluorescent protein

FBS
: fetal bovine serum

GXY
: glycine-X-Y

KD
: knockdown

NC1
: non-collagenous 1

OL
: overlay

RNAi
: RNA interference

RT-PCR
: reverse transcription-polymerase chain reaction

siRNA
: small interfering RNA

SS
: signal peptide sequence

Introduction

Basement membranes (BMs) are thin layers of the extracellular matrix surrounding epithelial tissues, nerves, muscles, fat cells, and blood vessels. BMs are supramolecular assemblies mainly composed of two independent self-assembling networks of collagen IV and laminin. These polymeric structures are interconnected by nidogen and heparan sulfate proteoglycans, perlecan, and agrin [1,2] and, in epithelial tissues, appear like sheets separating epithelial cells from the neighboring stroma, which serve as a mechanical scaffold for epithelial cell adhesion. In addition, BMs send pleiotropic signals to epithelial cells that regulate cell proliferation, survival, motility, polarization, and differentiation, thus being a critical determinant of epithelial function and morphology [3]. Although BMs appear to be static in homeostatic adult tissues, processes of BM formation, especially in early development and repair processes in organ regeneration, are essentially dynamic [4–6]. Recent evidence also suggests that dynamic BM deposition and rearrangement guide coordinated cellular behaviors to shape epithelial tissues [7]. On the other hand, abnormal BM dynamics is implicated to cause several pathological conditions, such as fibrosis [8] and cancer invasion [9].

Therefore, it is important to elucidate the underlying physiological and pathological mechanisms regulating BM formation and rearrangement in epithelial tissues. Previous efforts to understand these dynamic processes converge on the concept that laminin assembly is instructive for BM formation. At first, laminin is concentrated by cell surface receptors, such as dystroglycan and integrins [10–13], or by membrane lipid sulfatides [14]. This progressive concentration leads to the self-assembly of nascent laminin networks that are required for accumulating other BM components on the cell surface [15,16]. Nidogen and heparan sulfate proteoglycans can bind to both laminin and collagen IV, linking collagen IV to laminin networks. Collagen IV self-assembles into a network and becomes structurally reinforced with covalent crosslinks during the BM formation. This event stabilizes the BM and endows tissues, including the epithelium, with tensile strength [17–19]. Although much has been revealed, unanswered questions remain. BM components are secreted by both epithelial cells and the surrounding stromal cells [20]. In particular, stromal fibroblasts are implicated as the major sources of collagen IV which is incorporated in the epithelial BM in the intestine [21] and skin [22]. However, collagen IV is secreted as a large heterotrimeric complex and, once released outside the cell, the trimer may self-associate to form hexamers [23] or dodecamers [24], or interact with other BM components [25]. Combined with the self-assembling nature of collagen IV *in vitro* [26], it is puzzling why stroma-derived collagen IV travels to the distant epithelial BM region without forming insoluble aggregates en route. It is also unclear how secreted collagen IV is incorporated as an insoluble network in spatially confined BM regions.

In this study, we established an *in vitro* co-culture model of human colon epithelial cells and fibroblasts to reveal the dynamics of collagen IV assembly in epithelial BM formation. Our exclusive co-culture model, in which almost all collagen IV assembled in the BM-like structure at the base of

epithelial cells was supplied by fibroblasts, allowed us to specifically analyze and evaluate the collagen IV secreted by fibroblasts during the BM formation. We tested the varying degrees of fibroblast contribution by manipulating the co-culture configuration coupled with extensive microscopic observation, including live cell/BM imaging. As a result, we found unexpectedly active new roles of fibroblasts in the delivery and incorporation of collagen IV in the formation of epithelial BMs.

Results

Basement membrane-like structures are formed at the base of epithelial cells co-cultured with fibroblasts embedded in a collagen I gel

To investigate the dynamic processes of BM formation, *in vitro* cell culture is advantageous compared to the use of whole animals. First, we can specify the cellular sources of secreted BM proteins by selecting appropriate cell lines, which is difficult in animal tissues. Second, the cells and culture conditions can be easily modified. Third, the cells can be tracked under a microscope during analysis. Thus, we initially aimed to establish a culture system in which BMs are formed cooperatively by epithelial and stromal cells. DLD-1 human colon epithelial cells were cultured on top of a collagen I gel embedded with OUMS-36T-2 immortalized human embryonic fibroblasts (designated as 36T-2 cells hereafter) as stromal cells (Fig. 1A). This co-culture configuration represents the *in vivo* situation of epithelial tissue covering collagen-containing interstitial matrix. We used non-pepsinized type I collagen at a concentration of 2.1 mg/mL to make a gel. At this concentration, pore size between collagen fibers (or mesh size) was assumed to be 1–10 μm [27–29], which is comparable to the values estimated from the second harmonic generation images of loose connective tissue of human dermis and colon mucosa [29,30]. However, the composition of interstitial matrix differs depending on the body part and generally includes other fibrous proteins such as type III collagen and elastin. Therefore, it should be noted that our co-culture may not match with some tissue environments *in vivo*.

First, the entire gel containing DLD-1 and 36T-2 cells was fixed and fluorescently stained with anti-BM component antibodies and then observed under either a widefield microscope or a confocal laser scanning microscope. Laminin and collagen IV accumulated at the interface between DLD-1 cells and collagen I gel (Fig. 1B). We observed that BM proteins were deposited in extracellular regions, because immunostaining signals could be detected in samples without cell membrane permeabilization (Fig. 1C). The amounts of laminin and collagen IV increased gradually over time, reaching maximum levels at 4 days after the start of co-culture. Confocal microscopy clearly showed that these two BM components formed a thin sheet-like structure beneath DLD-1 cells, a characteristic of the BM (Fig. 1D). At high magnification, laminin and collagen IV appeared to form

independent fibrillar network structures that partially overlapped with each other, morphologically resembling developing intestinal BM *in vivo* [31] (Fig. 1D, right). Other BM components, such as nidogen-1 and perlecan, also colocalized with laminin networks (Fig. 1E). When DLD-1 cells were cultured on a collagen I gel without fibroblasts, only a trace amount of collagen IV was detected, while a certain amount of laminin was observed (Fig. 1F). Nidogen-1 and perlecan levels were also decreased. All the above data indicated that DLD-1 cells assembled BM-like structures in our co-culture, and the accumulation of collagen IV was crucially dependent on the activity of 36T-2 fibroblasts.

A large fraction of collagen IV in the BM-like structure is derived from 36T-2 fibroblasts

Collagen IV is encoded by six genes in humans (*COL4A1* to *COL4A6*), each corresponding to α1(IV) to α6(IV) chains. Among the many potential combinations, the chain composition of collagen IV heterotrimers found in mammals is limited to only three: α1α1α2, α3α4α5, and α5α5α6 [32]. To examine the sources of BM collagen IV in our co-culture, we first determined the expression levels of BM component genes in DLD-1 cells and 36T-2 cells by semi-quantitative reverse transcription PCR (RT-PCR) (Fig. 2). Among the six collagen IV genes, *COL4A1* and *COL4A2* were expressed in both DLD-1 and 36T-2 cells, whereas *COL4A3* and *COL4A5* were expressed only in 36T-2 cells. Of note, *COL4A4* and *COL4A6* were almost absent in both cell lines (Fig. 2; compare lanes 1 and 2 with the positive control lane 4), suggesting that collagen IV α1α1α2 was the sole heterotrimer species existing in the co-culture. As the transcripts used for RT-PCR were separately collected from independent cultures of DLD-1 cells and 36T-2 cells, it is possible that expression of some collagen IV genes was induced when these cells were co-cultured in collagen I gels. However, this was not the case because transcripts isolated from the co-culture showed almost no, if any, expression of *COL4A3* to *COL4A6* (Fig. 2, lane 3). Other BM components, laminin (*LAMA5* and *LAMC1*) and perlecan, were expressed in both cell lines, and nidogens (*NID1* and *NID2*) were expressed exclusively in 36T-2 cells.

Since collagen IV was not detected in the BM region when DLD-1 cells were cultured alone on collagen I gels (Fig. 1F), 36T-2 cells were presumably the main source of collagen IV during co-culture BM formation. To directly test this possibility, we knocked down the expression of collagen IV only in 36T-2 cells by transfection with small interfering RNAs (siRNAs) prior to the start of co-culture. First, we confirmed the efficient reduction of *COL4A1* and *COL4A2* levels by RNA interference (RNAi) in 36T-2 cells (Fig. 3A). Then, DLD-1 cells were co-cultured with these siRNA-treated 36T-2 cells and the accumulation of BM components on day 4 was measured by immunofluorescence signal intensities. Strikingly, the amount of collagen IV was reduced by 74% in the co-culture using siCOL4A1-treated 36T-2 cells, and by 63% in siCOL4A2-treated 36T-2 cells, compared to the control (Fig. 3B and C). There were no changes in the amount of laminin. However, laminin network formation seemed disturbed, as seen in the increase of dot-like patterns of laminin

distribution in the condition using collagen IV-knockdown (KD) 36T-2 cells (Fig. 3B, bottom panels). Nidogen-1 and perlecan accumulated in the BM region at slightly reduced levels when COL4A1 was knocked down in 36T-2 cells, compared to the control (Fig. 3C, D, and E). For both proteins, similar structural changes from network to dot-like patterns were observed, as in the case of laminin (Fig. 3D and E, insets). All these results demonstrated that in our co-culture, collagen IV in the BM was derived mostly from 36T-2 fibroblasts and suggest that collagen IV is dispensable for the accumulation of other BM components but structurally required to enhance BM network structures.

As an inverse experiment, we knocked down collagen IV only in DLD-1 cells and co-cultured them with non-treated 36T-2 cells. Under these conditions, the amount of BM collagen IV showed no difference from the control (Fig. 3B and C), further showing that almost all the BM collagen IV in this co-culture originated from 36T-2 cell secretion. Although DLD-1 cells expressed the *COL4A1* and *COL4A2* transcripts (Fig. 2), the protein products were probably not secreted outside the cell.

In our co-culture, laminin deposition at the base of DLD-1 cells was a pre-requisite for the recruitment of 36T-2-derived collagen IV in the BM region, as shown by laminin KD experiments (Fig. 4). To inhibit laminin secretion in the co-culture, we knocked down laminin γ1 (encoded by *LAMC1*), an essential subunit of laminin heterotrimers to organize laminin network structures [33] (Fig. 4A). Laminin signals at the base of DLD-1 cells were successfully suppressed only when both 36T-2 and DLD-1 cells were treated with siLAMC1 (Fig. 4B), indicating that BM laminin in the co-culture originated from both epithelial and fibroblast sources. Quantification of laminin immunofluorescence after 4 days in the BM region of the KD co-culture showed 63% reduction compared to that of the control (Fig. 4C). The levels of collagen IV and nidogen-1 accumulation in the KD co-culture were correspondingly reduced by 67% and 62%, respectively, compared to the control levels (Fig. 4B and C), which is consistent with the widely recognized role of laminin as an initiator of BM formation [15,16].

BM Collagen IV is deposited by 36T-2 fibroblasts in proximity to DLD-1 epithelial cells

The predominant contribution of 36T-2 cells in BM collagen IV assembly in our co-culture enabled us to examine the dynamic behavior of collagen IV during BM formation. First, we searched for the proper location of enhanced green fluorescent protein (EGFP) tagging in COL4A1 protein (Fig. 5A). As reported previously for invertebrate collagen IV [34,35], a construct containing EGFP just after the signal peptide of COL4A1 (32Ala in Fig. 5A and B; hereafter designated as EGFP-COL4A1) was found to behave similarly to endogenous collagen IV (Fig. 5B and C). To visualize collagen IV derived from a single fibroblast source, 36T-2 cells stably expressing EGFP-COL4A1 were mixed with wild-type cells at a 1:20 ratio, and the mixtures were co-cultured with DLD-1 cells. Interestingly, EGFP-COL4A1 was detected only in restricted areas within the BM-like structure, and cell bodies of

EGFP-COL4A1-expressing 36T-2 cells were frequently found nearby (Fig. 5D). This observation suggested that 36T-2 cell-derived collagen IV was incorporated into the BM-like structure only when 36T-2 cells approached the basal surface of epithelial cells. To test this, 36T-2 cells were kept approximately 1 mm away from DLD-1 cells at the start of co-culture by overlaying an additional cell-free collagen I gel on the 36T-2 cell-containing gel (Fig. 6A). When 2.1 mg/mL collagen I gel was overlaid, collagen IV that accumulated in the BM region after 4 days of co-culture was reduced by 82% compared to the condition without the additional gel layer (Fig. 6B and C). Instead, the soluble collagen IV that presumably failed to assemble in the BM region was increased in the culture medium collected from the condition with a gel layer (Fig. 6D). The laminin level with an additional gel layer showed no decrease, compared to that without a gel layer. Interestingly, the level of nidogen-1, which was mostly secreted by 36T-2 cells as was collagen IV (Fig. 2), significantly decreased but remained at 73% of that of control. We also tested overlaying 1.3 mg/mL collagen I gel whose pore size between fibers was expected to expand [28], thus enabling faster macromolecular diffusion within a gel [36]. Accordingly, nidogen-1 accumulation in the BM region slightly restored to the level of 91% of the control value. However, collagen IV was still strongly inhibited to accumulate at the BM region, regardless of collagen concentration of the additional layer (Fig. 6B and C). These data suggested that collagen IV was unlikely to be delivered to the BM region via molecular diffusion within a gel but was increasingly incorporated into the BM when 36T-2 cells were in proximity to the basal surface of DLD-1 cells.

Soluble collagen IV in the co-culture media appeared to be inefficient in being integrated into insoluble networks in the BM region, since a significant amount of secreted collagen IV was detected in the culture media (Fig. 6D). This was also implicated in a previous report on alveolar epithelial cells [37]. Thus, we hypothesized that direct contact or close apposition of fibroblasts to the base of epithelia facilitates BM collagen IV deposition by fibroblasts. To test this hypothesis, we used Transwell chambers with three different cell topologies: one in which DLD-1 cells were seeded on the top side of the Transwell membrane with high pore density and 0.4 μm pore diameter, and 36T-2 cells were seeded in the lower well (Fig. 7A, (i)). This allows collagen IV to reach the BM region only by diffusion and convection. Another in which 36T-2 cells were seeded on the undersurface of the membrane, in which the local concentration of collagen IV near the BM region is expected to increase, especially within the membrane pores, but direct contact between 36T-2 cells and DLD-1 cells is presumably prohibited (Fig. 7A, (ii)). In the third, in addition to the first topology, a small number of 36T-2 cells were pre-seeded before the top surface of the membrane was seeded by DLD-1 cells, which allowed direct contact between the two (Fig. 7A, (iii)). After 4 days of co-culture with these topologies, collagen IV immunofluorescence showed that only a small amount of collagen IV accumulated at the base of DLD-1 cells in the first and second conditions, which did not allow direct contact. In contrast, intense fibrous collagen IV developed around the interface between DLD-1 cells and intermingled

36T-2 cells in the third condition (Fig. 7A, arrowheads). Nidogen-1 not only colocalized with these fibers but could be detected with the laminin aggregates which were largely devoid of collagen IV (Fig. 7A, the boxed area), thus suggesting that nidogen-1 was capable of being incorporated into the BM via diffusion and/or convection. We confirmed the presence of a plenty of soluble collagen IV in the lower-well culture media in all the conditions (Fig. 7B). Therefore, it was likely that BM collagen IV was deposited by the 36T-2 cell population positioned close enough to touch the basal surface of DLD-1 cells.

36T-2 fibroblasts deposit Collagen IV as aggregates and rearrange them into fibril-like structures

To further analyze how 36T-2 cells deposit BM collagen IV, we performed live cell imaging of the co-culture using three-dimensional confocal microscopy. We used the EGFP-COL4A1-expressing 36T-2 stable cell line, which enabled us to visualize not only secreted collagen IV, but also cell bodies. To identify the position of DLD-1 cells simultaneously in co-culture, we labeled the nuclei by stably expressing histone H2B-mCherry in DLD-1 cells. In the time window from day 3 to day 4 of the co-culture, we could reproducibly observe collagen IV aggregates and fibril-like structures that were similar in size to those seen in Fig. 1B, at the basal region of DLD-1 cells. During 15 hours of analysis, migrating 36T-2 cells frequently left collagen IV aggregates behind when they approached within several microns from the basal surface of DLD-1 cells (Fig. 8A and Movie S1). Once deposited, these aggregates remained in the BM region and appeared to adhere to the BM-like structure. Interestingly, collagen IV aggregates were often extended and transformed into long fibrils, seemingly due to the traction force exerted on one end of the aggregates by proximally migrating 36T-2 cells (Fig. 8B and Movie S2). In addition, we observed irregular displacements of each aggregate and fibril in the plane of the BM region. These movements appeared to be independent of the movement of overlaying DLD-1 cells (see the movement of DLD-1 nuclei in Movie S1, lower left region), implying a dominant effect of 36T-2 cells in rearranging BM collagen IV networks. Overall, the above results indicated that fibroblasts deposit collagen IV aggregates that can be incorporated into the BM region and further rearrange such aggregates into fibrous networks by physically associating with them.

36T-2 cells occasionally deposited collagen IV aggregates near the collagen I gel surface not covered by DLD-1 cell sheets (Fig. 8C and Movie S3). However, these aggregates were immediately captured by other 36T-2 cells passing near the aggregates, suggesting a retrieval and/or recycling mechanism for abnormally deposited collagen IV during BM formation.

36T-2 cell motility is required for efficient BM collagen IV assembly

We have demonstrated that fibroblast-derived collagen IV is efficiently incorporated into the BM only when fibroblasts come close to the basal surface of epithelial cells. To assemble a

homogenous sheet-like BM with uniform collagen IV distribution, it was assumed that fibroblasts should be sufficiently motile within collagen I gels. To examine the role of fibroblast migration in BM collagen IV assembly, we attenuated 36T-2 cell motility by transfecting siRNAs targeting *WAVE2* or *NCKAP1*, both of which are critical regulators of cell motility within three-dimensional substrates by activating the Arp2/3 complex [38,39]. We also examined the effect of α-actinin-1 (*ACTN1*) KD, which regulates cell motility by a mechanism different from that of Arp2/3 activators. α-actinin-1 is known to stabilize focal adhesions [40] and enhance cell motility within collagen I gels [41]. Knockdown of each of these proteins in 36T-2 cells was confirmed (Fig. 9A), and the respective siRNA-treated cells were suspended in collagen I gels and co-cultured with DLD-1 cells. As assumed, 36T-2 cells treated with WAVE2, NCKAP1 or ACTN1 siRNAs exhibited decreased accumulation of BM collagen IV compared with siControl-treated cells (Fig. 9B and C). The laminin levels between the four conditions were similar. These data were in line with the notion that fibroblast motility is required for the efficient incorporation of collagen IV into the BM. However, the amount of soluble collagen IV in culture media collected from co-culture of siACTN1-treated 36T-2 cells was slightly reduced compared to that in the other three (Fig. 9D), suggesting that the decrease in BM collagen IV observed for siACTN1-treated 36T-2 cells might partially reflect the reduction in collagen IV secretion. Nevertheless, the results further support our findings that fibroblasts contribute to the formation of epithelial BMs in the limited region proximal to the basal surface of epithelial cells.

Discussion

In this study, we found that the proximal interaction between fibroblasts and epithelial cells is critical for the incorporation and rearrangement of collagen IV during BM formation. Our *in vitro* co-culture system suggests that collagen IV molecules diluted in the culture media are not efficiently incorporated into the BM, but rather only those secreted by fibroblasts in close proximity (within several microns) can be involved in BM formation. We propose some possible mechanisms by which collagen IV trimers can form insoluble aggregates or fibril-like structures, specifically in the BM region.

First, the limited diffusion of collagen IV trimers within fibrillar networks of collagen I gels promotes polymerization and insolubilization. The concentration of the collagen I used in this study was 2.1 mg/mL. At this concentration range, diffusion of large molecules within collagen I gels is thought to be significantly impeded [36]. Actually, the diffusion of collagen IV appeared to be hindered even in a diluted 1.3 mg/mL gel (Fig. 6B and C). It is known that the length of the collagen IV trimer is extended up to ~400 nm, the longest among BM macromolecules [42]. In addition, collagen IV trimers are prone to self-assemble to form hexamers, dodecamers, and possibly oligomers of more monomers, in the extracellular environment [23,32]. Therefore, collagen IV diffusion is thought to be

extremely limited to the narrow space around cell bodies that secrete collagen IV. This raises the local concentration of collagen IV to a level above the critical concentration for polymerization, allowing collagen IV to be deposited only proximal to the cellular origin. In contrast, Nidogen-1 is much smaller with a size of about 20 nm [42] or a Stokes radius of 6.8 nm [43], which presumably permits Nidogen-1 to reach the BM region by diffusion as shown in Fig. 6B and C. Although the pore size of fibrous ECM network is one of the most important parameters that determine the diffusive and rheological properties [36,44], the pore size of interstitial matrix *in vivo* is largely unknown partly due to the complexity of the composition which includes a variety of fibrous proteins and sugar chains in addition to collagens. However, in the small intestine, Granger *et al.* estimated the pore size of interstitial matrix to be ~100 nm [45], suggesting that hindrance of diffusion and convection of collagen IV trimers could occur *in vivo*. In this scenario, collagen IV can accumulate not only in the BM but also in other stromal regions. However, we speculate that such ectopically deposited collagen IV is unstable and subject to digestion by collagenolytic enzymes [46] or retrieval/recycling by other cells, as shown in Fig. 8C. Remarkably, it has been reported that the urokinase plasminogen activator receptor-associated protein (uPARAP)/Endo180 is expressed in fibroblasts and functions as a collagen IV receptor for cellular uptake [47].

Second, we propose a mechanism in which collagen IV is deposited first on the fibroblast cell surface as an insoluble aggregate, which is then transported together by the fibroblasts as they migrate toward the BM. Once they reach the BM, fibroblasts shed off some of the collagen IV they carry by making physical contact with the BM, as implicated in the live imaging data (Fig. 8). For this to occur, secreted collagen IV must be attached to the fibroblast cell surface, which is quite possible because fibroblasts generally express adhesion receptors for collagen IV, namely integrins $\alpha 1\beta 1$ and $\alpha 2\beta 1$ [48,49]. Collagen IV aggregates attached to the fibroblast cell surface could be released if the aggregates have higher avidity for preexisting BM components at the basal surface of epithelial cells. This could happen when considering the high-affinity interaction between collagen IV and nidogens [1]. A slight increase in the amount of collagen IV in nascent BMs would accelerate collagen IV accumulation via its self-associating ability. Integrins in epithelial cells might also be involved in collagen IV recruitment, as observed in *C. elegans* larvae [50]. All these interactions hold collagen IV aggregates in the BM region. Interestingly, it has been reported that collagen VI, another type of network-forming collagen, remains associated with the cell surface of cultured tendon fibroblasts after secretion and is deposited preferentially at the cell periphery to form insoluble aggregates [51]. A similar mode of deposition may occur in the case of collagen IV, but it could be possible that fibroblasts directly deposit collagen IV fibril-like structures onto the BM through the fibripositor-like structure, as reported for type I collagen of chick tendon [52].

These mechanisms may be involved *in vivo*. In *Drosophila* embryos, local deposition of collagen IV was observed during ventral nerve cord development [53]. In this process, highly motile

BM component-secreting cells called hemocytes locally deposit collagen IV, while laminin is dispersed over a distance from hemocytes, similar to the results obtained in our *in vitro* study. In contrast, during *Drosophila* larval development, collagen IV appears to be diffused from fat bodies to distant organs [54]. Likewise, it has been reported in *C. elegans* larvae that BM collagen IV in the pharynx and intestine is supplied by distantly located body wall muscle cells [55]. Thus, whether BM collagen IV accumulates either via local deposition or by collecting diffusive molecules seems to depend on the location of the BM-forming tissues. In the above cases, diffusive collagen IV appears to be transported through fluid-filled body cavities, such as the hemolymph for *Drosophila* and the pseudocoelom for *C. elegans*. However, vertebrate epithelial cells generally accompany the interstitial matrix, which contains fibrillar collagens and glycosaminoglycans, adjacent to the basal surface, and thus diffusion-mediated delivery of BM components is unlikely to occur. Alternatively, solubility and effective diffusion of vertebrate collagen IV can be enhanced by collagen-binding proteins such as secreted protein acidic and rich in cysteine (SPARC), as demonstrated mainly in invertebrates. However, the impact of SPARC in vertebrate BM assembly may not be as prominent as that of invertebrates because SPARC and its homolog SPARCL1/Hevin proteins are not detectable in collagen IV-rich BMs of some epithelial tissues [32], and SPARC and SPARCL1 double-null mice survive into adulthood [56]. Therefore, fibroblast-mediated proximal deposition could be a significant mode of collagen IV assembly in vertebrate epithelial BMs.

In this study, fibroblast motility was not only required for the deposition of BM collagen IV but also involved in rearrangement of the preexisting networks. Contrarily, the movement of DLD-1 cells seemed irrespective of the direction of rearranging collagen IV fibril-like structures (Movie S1), suggesting that epithelial cell motility might be less significant in the rearrangement phase. However, the importance of epithelial cell motility was highlighted in the BM laminin assembly in MCF10A cells [57] and the polarized alignment of collagen IV fibril-like structures in the BM of *Drosophila* follicular epithelial cells [58]. As a whole, the relationship between epithelial cell motility and BM formation remains incompletely understood and needs further investigation.

Close apposition of epithelial cells and fibroblasts is prevalent in many organs, including the intestine [59], lungs [60], renal tubules [61], and hair follicles [62]. For example, the stroma of small intestinal crypts and villi contains several types of stromal cells, including fibroblast and myofibroblast subtypes. Some of these cells make broad contact and adhere to the BM just below the epithelium [63]. Similar adhesions can also be observed in other organs. Interestingly, collagen IV isoforms in the intestinal BM are differentially distributed from the crypt base to the top of the villus [64]: α1α1α2 is exclusively enriched in the crypt and all the isoforms can be detected at the villus, whereas α1α1α2 and α5α5α6 but not α3α4α5 are detectable in the transition zone between them. In addition, different subsets of stromal cell types populate a certain length of the stroma along the crypt-villus axis. Thus, a combination of collagen IV isoforms expressed in each cellular subset may dictate

the differential localization of isoforms in the intestinal BM, in which we can envision proximal deposition of collagen IV by fibroblasts at work *in vivo*. If the intimate epithelium-fibroblast association is broken by pathological conditions, such as inflammation or precancerous conditions, the BM organization can be disturbed, which may lead to epithelial tissue disorganization. Definitely, our study not only contributes to explain the biological mechanistic insight of the BM assembly, but it also could be useful to understand the pathological processes in different BM diseases.

Materials and methods

Cells and cell culture

Human epithelial colorectal adenocarcinoma cell line (DLD-1) and human mammary gland epithelial cell line (MCF10A) were obtained from the American Type Culture Collection (CCL-221 and CRL-10317, ATCC, Manassas, VA, USA). Human embryonic fibroblasts (OUMS-36T-2 cells) were obtained from the Japanese Collection of Research Bioresources Cell Bank (JCRB1006.1, JCRB, Osaka, Japan). Cells, except for MCF10A cells, were cultured in Dulbecco's modified Eagle's medium (DMEM; 041-29775, Wako, Osaka, Japan) supplemented with 10% fetal bovine serum (FBS). MCF10A cells were cultured using MEGM mammary epithelial cell growth medium BulletKit (CC-3150, Lonza, Basel, Switzerland). Cells were maintained at 37 °C under a humidified atmosphere of 5% CO_2.

Collagen I gel co-culture

2.1 mg/mL collagen I gel solution was prepared by mixing the following solutions at a volume ratio of 7:2:1 on ice: Cellmatrix Type I-A (3.0 mg/mL collagen type I acid-extracted from porcine tendon; Nitta Gelatin, Osaka, Japan); 5× DMEM (DMEM powder was dissolved in water; 05915, Nissui, Tokyo, Japan); reconstitution buffer (260 mM $NaHCO_3$, 200 mM HEPES and 50 mM NaOH). To prepare 1.3 mg/mL collagen I gel for overlay experiments (Fig. 6), Cellmatrix Type I-A solution was diluted to 1.86 mg/mL by mixing with cold 1 mM HCl just prior to use and neutralized as described above.

In 130 µL of 2.1 mg/mL collagen I gel solution on ice, 4.0×10^4 cells of 36T-2 cells were suspended and applied to the bottom well of a glass-bottom dish (D11130H, Matsunami Glass, Osaka, Japan). The solution was then allowed to gelate at 37 °C for 30 min. For overlay experiments, 200 µL cell-free collagen I solution was overlaid at this point and incubated for further 30 min. For co-culture, 2×10^5 cells of DLD-1 cells were suspended by 500 µL of DMEM with 10% FBS and placed on the surface of the gel. After the DLD-1 cells adhered to the surface of collagen I gel by overnight incubation, the culture medium was changed to DMEM with 10% FBS and 432 µM L-ascorbic acid 2-phosphate sesquimagnesium salt hydrate (AA2P; nacalai tesque, Kyoto, Japan) was added to ensure

proper collagen synthesis. The culture medium was replaced with fresh medium on the second day.

Transwell co-culture

Transwell co-culture was performed using the 24-well format Transwell inserts (polycarbonate membrane, 0.4 μm pore diameter; 3413, Corning, NY, USA). For the condition (i) (see Fig. 7A), 1.0×10^5 cells of 36T-2 cells were seeded in the lower well. 2.0×10^4 cells of DLD-1 cells were seeded on the porous membrane of the insert. After overnight incubation, the insert was placed in the 36T-2 cell-seeded lower well, and the culture medium was changed to DMEM with 10% FBS and 432 μM AA2P. For the condition (ii), 3.9×10^4 cells of 36T-2 cells were seeded on the undersurface of the Transwell membrane by turning the insert upside-down. After 5 h of incubation, the insert was placed in a 24-well plate well and 2.0×10^4 cells of DLD-1 cells were seeded on the upper surface of the membrane. After overnight incubation, the culture medium was changed to DMEM with 10% FBS and 432 μM AA2P. For the condition (iii), 2.0×10^2 cells of 36T-2 cells were pre-seeded on the Transwell membrane. After 5 h of incubation, the procedures for the condition (i) were performed as described above.

The cells were cultured for four days. The culture medium was replaced with fresh medium on the second day.

Immunofluorescence microscopy

Collagen I gels containing cells were fixed with 1% paraformaldehyde in 0.1 M HEPES-NaOH (pH 7.5) for 20 min at room temperature on a glass-bottom dish with gentle rocking. After fixation, gels were isolated from the glass-bottom dish and rinsed twice with PBS containing 30 mM glycine (G-PBS). Then, the gels were permeabilized by treating them with 0.2% Triton X-100 in G-PBS for 15 min. After washing thrice for 10 min with G-PBS, gels were incubated with primary antibodies for 2 h, followed by incubation with secondary antibodies for 90 min at room temperature. The antibody reaction was performed with gentle agitation.

Cells on coverslips were fixed with 10% ice-cold trichloroacetic acid in water for 10 min. Cells co-cultured using Transwell inserts were fixed with 1% paraformaldehyde in 0.1 M HEPES-NaOH (pH 7.5) for 15 min at room temperature. They were permeabilized by treatment with 0.2% Triton X-100 in G-PBS for 10 min and immunostained conventionally by incubation with primary antibodies for 1 h and secondary antibodies for 40 min at room temperature.

All stained samples were mounted with PermaFluor Aqueous Mounting Medium (TA-030-FM, Thermo Scientific, Waltham, MA, USA). Epifluorescence micrographs were taken with Olympus BX51 microscope with a UPlanFL N 20×/NA0.50 dry lens and a PlanApo 60×/NA1.40 oil lens (Olympus, Tokyo, Japan). Confocal micrographs were taken with an A1 confocal laser scanning microscope with a PlanApo N 40×/NA0.95 dry objective lens (Nikon, Tokyo, Japan).

The following primary antibodies were used: anti-human collagen IV mouse monoclonal antibody (1:500; F-59, Kyowa Pharma Chemical, Toyama, Japan), anti-collagen IV goat polyclonal antibody (1:500; AB769) and anti-laminin rabbit polyclonal antibody (1:1000; L9393) from Merck (Darmstadt, Germany), anti-perlecan rat monoclonal antibody (1:500; sc-33707) and anti-Scrib goat polyclonal antibody (1:200; sc-11049) from Santa Cruz Biotechnology (Dallas, TX, USA), anti-nidogen-1 mouse monoclonal antibody (1:300; MAB2570, R&D Systems, Minneapolis, MN, USA), and anti-GFP rabbit polyclonal antibody (1:1000; 598, MBL, Tokyo, Japan). The following antibodies were purchased from Thermo Fisher Scientific (Waltham, MA, USA) and used as secondary antibodies at 1:300 dilution: Alexa Fluor 488-conjugated (AF488) donkey anti-mouse IgG (H+L) (A21202), AF488 donkey anti-goat IgG (H+L) (A32814), AF488 donkey anti-rat IgG (H+L) (A21208), AF555 donkey anti-rabbit IgG (H+L) (A31572), AF555 donkey anti-mouse IgG (H+L) (A31570), and AF555 goat anti-rat IgG (H+L) (A21434), and AF647 donkey anti-goat IgG (H+L) (A21447). Cell nuclei were stained with 0.2 μg/mL DAPI (D212, Dojindo, Kumamoto, Japan). Actin filaments were stained with AF647 phalloidin (1:300; A22287, Thermo Fisher Scientific).

RNAi

siGENOME Non-Targeting Control siRNA Pool #2 and the siRNA targeting human *NCKAP1* (siGENOME SMARTpool) were purchased from Horizon Discovery (Cambridge, UK). siRNAs targeting human *COL4A1*, *COL4A2* and *LAMC1* were purchased from Hokkaido System Science (Sapporo, Japan). We designed two to four siRNAs targeting different regions of each gene. Among them, the sequence with minimal off-target effects and sufficient KD efficiency was chosen for further experiments. The selected siRNA target sequences were as follows: 5'-CACTAAAAGTCTCCAAAACAT-3' for siCOL4A1, 5'-GACCTTTCTAGACATCATTGT-3' for siCOL4A2, and 5'-GAGAATGAAGCAAATAACATA-3' for siLAMC1. The sequences for siWAVE2 and siACTN1 were previously described [39,40]. Each siRNA was transfected into cells using Lipofectamine RNAiMAX reagent (Thermo Fisher Scientific). siCOL4A1, siCOL4A2, or siLAMC1 was used at 20 nM. siWAVE2, siNCKAP1, or siACTN1 was used at 10 nM. To obtain sufficient levels of suppression by RNAi, a second transfection was carried out 12 h after the first. The double-transfected cells were cultured in DMEM with 10% FBS for 12 h before being embedded into collagen gels as described above. For RT-PCR analysis, the double-transfected cells were cultured for 36 h before RNA isolation.

RT-PCR

Total RNA was isolated with ISOGEN (319-90211, NIPPON GENE, Tokyo, Japan), following the manufacturer's instructions. For RNA isolation from co-culture collagen I gel, NucleoSpin RNA kit (740955, Takara Bio, Shiga, Japan) was used according to the manufacturer's

instructions. cDNA synthesis was performed using ReverTra Ace (TRT-101, TOYOBO, Osaka, Japan). Each reaction mixture contained 1 μg of total RNA, 50 U ReverTra Ace, 2 μM primer mix (TOYOBO) and 0.2 mM dNTPs in 10 μL reaction buffer. PCR was performed using KOD-ONE PCR master mix (KMM-201, TOYOBO). 1 μM each of forward and reverse gene-specific primers was used in a final volume of 20 μL. For each reaction, 0.1 μL of the synthesized cDNA was used, except for the co-culture condition (Fig. 2), in which 0.2 μL of the cDNA was used. Gene-specific primer sequences are listed in Table 1. The number of cycles for PCR were chosen to be the linear range of amplification (Table 1). The PCR products were electrophoresed in a 1.5% agarose gel and visualized with ethidium bromide using UV illumination.

Western blotting

The culture supernatant was collected and centrifuged at 2,000 rpm for 5 min to remove floating cells. The supernatant was mixed with 4× Laemmli sample buffer at a ratio of 3:1, and boiled at 95 °C for 5 min. Western blotting was performed using standard procedures. Electrophoresis was performed using 4%–15% Mini-PROTEAN TGX gel (4561086, Bio-Rad, Hercules, CA, USA). Anti-collagen IV goat polyclonal antibody (1:1500; Merck), anti-laminin rabbit polyclonal antibody (1:3000; Merck) and anti-nidogen-1 mouse monoclonal antibody (1:2000; R&D Systems) were used as primary antibodies, followed by detection with alkaline phosphatase (AP)-conjugated donkey anti-goat IgG (1:5000; V1151, Promega, Madison, WI, USA), goat anti-rabbit IgG (1:5000; S3731) and goat anti-mouse IgG (1:5000; S3721), respectively.

Construction of EGFP-COL4A1

A full-length human COL4A1 fragment (5010 bp including the start/stop codons) was amplified by PCR using the MCF10A cell cDNA as a template. The forward and reverse primers for COL4A1 amplification were flanked by BglII and SalI sites, respectively. The PCR product was cloned into the BglII/SalI sites of pCMV5 vector, and direct sequencing confirmed human COL4A1 sequence. Then, the COL4A1 fragment was excised by BglII/SalI and subcloned into the BamHI/XhoI sites of the mammalian expression vector pcDNA 3.1 (+). An EGFP fragment was inserted into the intermediate site of COL4A1 by In-Fusion HD cloning kit according to the manufacturer's instructions (Z9648N, Takara Bio). Insertion sites of EGFP were indicated in Fig. 5A. There are 21 short non-collagenous interruptions in the GXY repeat sequence of COL4A1, which confer flexibility to rigid collagenous triple helices and thus provide potential insertion sites that do not interfere with heterotrimer formation. These sites were used in 641Ile and 940Lys constructs. For EGFP insertion at the C-terminus of COL4A1, a full-length human COL4A1 fragment except for the stop codon was amplified by PCR and inserted into the BglII and SalI sites of pEGFP-N3 vector. The sequence was confirmed by direct sequencing.

Generation of stable cell lines

36T-2 cells were transfected with pcDNA-EGFP-COL4A1 (32Ala, see Fig. 5A), and DLD-1 cells were transfected with pmCherry-N1-histone H2B (H2BC3; cloned from MCF10A cDNA) using Lipofectamine 2000 reagent (Thermo Fisher Scientific). Single colonies were isolated after 10-14 days of G418 selection (600 μg/mL for 36T-2 cells, 400 μg/mL for DLD-1 cells; 078-05961, FUJIFILM Wako, Osaka, Japan). EGFP-COL4A1 expression was assessed by immunofluorescence using an anti-GFP antibody.

Live-cell imaging

Histone H2B (H2B)-mCherry stably expressing DLD-1 cells were co-cultured for 3 days on the type I collagen gel embedded with EGFP-COL4A1 stably expressing 36T-2 cells. Prior to the start of live-cell imaging, the medium was replaced with DMEM supplemented with 10% FBS, 432 μM AA2P and 0.3 mM Trolox (238813, Merck). Time-lapse microscopic observations were performed using an A1 confocal laser scanning microscope equipped with a Plan Apo λD 20×/NA0.8 lens (Nikon) and a stage-top incubator system (37 °C, humidified, 5% CO_2; Tokai Hit, Shizuoka, Japan). Images were taken as one frame every 10 min for 15 h. Each image was acquired as z-stack with 4 μm steps and at least 10 slices. The slices that were best-focused at the BM region were manually chosen for each time point and processed to a movie using Fiji Image J software.

Quantification of immunofluorescence micrographs

All immunofluorescence images were analyzed using the Fiji ImageJ software. The same acquisition settings were used for all the images taken for each protein. For each epifluorescence micrograph, the total fluorescence intensity was measured in the region where laminin network structures were in focus. We excluded the area from measurement that contained signals of the cell body of 36T-2 cells. The background signal was measured at the epithelial cell region where the BM-like structure was out of focus. The total fluorescence intensity of the image was corrected by subtracting the background intensity. Three microscopic regions per sample was quantified and averaged to get the fluorescence value of one experiment. For confocal micrographs, three slices of the basal region of DLD-1 cells were reconstructed to an average-intensity-projection image. This image was used for calculation of the fluorescent intensity as described for epifluorescence micrographs.

Statistical analysis

Statistical analyses were performed using Microsoft Excel for Office 365. All experiments were independently repeated at least three times. The means of the values of 3–7 independent

experiments were calculated accompanying standard errors (SEs). Statistical significance was assessed using unpaired two-sided Student's *t*-test. Differences in means were considered statistically significant at $p < 0.05$, or $p < 0.01$, as indicated in the figures.

Acknowledgements

We thank all the members of our laboratory for help and advice throughout this study. We also thank Tokushima Bioimaging Station (T-BIS, Tokushima University) for assistance in microscopy, and Support Center for Advanced Medical Sciences (Tokushima University) for experimental assistance. This study was supported by JSPS KAKENHI Grant Numbers 20J14688 to AyT, 25860215 and 18K06932 to SK, and 26650071, 15KT0086 and 18H02617 to SY, by Grant from the Japan Science and Technology Agency (JST) under grant number JPMJMS2022 to SY, and by JST CREST Grant Number JP115811 to SY.

Author contributions

SK and SY designed the study; AyT, SK, KS, and TN performed experiments; AyT and SK analyzed data; AyT, SK, KS, TN, AkT, and SY contributed to discussion; AyT and SK wrote the draft; SK and SY reviewed and edited the paper.

References

1 Yurchenco PD (2011) Basement membranes: cell scaffoldings and signaling platforms. *Cold Spring Harb Perspect Biol* **3**, a004911.

2 Timpl R & Brown JC (1996) Supramolecular assembly of basement membranes. *Bioessays* **18**, 123–132.

3 Sekiguchi R & Yamada KM (2018) Basement membranes in development and disease. *Curr Top Dev Biol* **130**, 143–191.

4 Bonnans C, Chou J & Werb Z (2014) Remodelling the extracellular matrix in development and disease. *Nat Rev Mol Cell Biol* **15**, 786–801.

5 Morrissey MA & Sherwood DR (2015) An active role for basement membrane assembly and modification in tissue sculpting. *J Cell Sci* **128**, 1661–1668.

6 Wilson SE, Marino GK, Torricelli AAM & Medeiros CS (2017) Injury and defective regeneration of the epithelial basement membrane in corneal fibrosis: A paradigm for fibrosis in other organs? *Matrix Biol* **64**, 17–26.

7 Khalilgharibi N & Mao Y (2021) To form and function: on the role of basement membrane mechanics in tissue development, homeostasis and disease. *Open Biol* **11**, 200360.

8 Decaris ML, Gatmaitan M, FlorCruz S, Luo F, Li K, Holmes WE, Hellerstein MK, Turner SM & Emson CL (2014) Proteomic analysis of altered extracellular matrix turnover in bleomycin-induced pulmonary fibrosis. *Mol Cell Proteomics* **13**, 1741–1752.

9 Fiore VF, Krajnc M, Quiroz FG, Levorse J, Pasolli HA, Shvartsman SY & Fuchs E (2020) Mechanics of a multilayer epithelium instruct tumour architecture and function. *Nature* **585,** 433–439.

10 Vandenberg P, Kern A, Ries A, Luckenbill-Edds L, Mann K & Kuhn K (1991) Characterization of a type IV collagen major cell binding site with affinity to the α1β1 and the α2β1 integrins. *J Cell Biol* **113**, 1475–1483.

11 Hall DE, Reichardt LF, Crowley E, Holley B, Moezzi H, Sonnenberg A & Damsky CH (1990) The alpha 1/beta 1 and alpha 6/beta 1 integrin heterodimers mediate cell attachment to distinct sites on laminin. *J Cell Biol* **110**, 2175–2184.

12 Kikkawa Y, Sanzen N & Sekiguchi K (1998) Isolation and characterization of laminin-10/11 secreted by human lung carcinoma cells: Laminin-10/11 mediates cell adhesion through intergrin αβ1. *J Biol Chem* **273**, 15854–15859.

13 Henry MD & Campbell KP (1998) A role for dystroglycan in basement membrane assembly. *Cell* **95**, 859–870.

14 Li S, Liquari P, McKee KK, Harrison D, Patel R, Lee S & Yurchenco PD (2005) Laminin-sulfatide binding initiates basement membrane assembly and enables receptor signaling in Schwann cells and fibroblasts. *J Cell Biol* **169**, 179–189.

15 Hohenester E & Yurchenco PD (2013) Laminins in basement membrane assembly. *Cell Adh Migr* **7**,

56–63.

16 Sasaki T, Fässler R & Hohenester E (2004) Laminin: The crux of basement membrane assembly. *J Cell Biol* **164**, 959–963.

17 Pöschl E, Schlötzer-Schrehardt U, Brachvogel B, Saito K, Ninomiya Y & Mayer U (2004) Collagen IV is essential for basement membrane stability but dispensable for initiation of its assembly during early development. *Development* **131**, 1619–1628.

18 McCall AS, Cummings CF, Bhave G, Vanacore R, Page-Mccaw A & Hudson BG (2014) Bromine is an essential trace element for assembly of collagen IV scaffolds in tissue development and architecture. *Cell* **157**, 1380–1392.

19 Isabella AJ & Horne-Badovinac S (2015) Dynamic regulation of basement membrane protein levels promotes egg chamber elongation in *Drosophila*. *Dev Biol* **406**, 212–221.

20 Brown NH (2011) Extracellular matrix in development: Insights from mechanisms conserved between invertebrates and vertebrates. *Cold Spring Harb Perspect Biol* **3**, a005082.

21 Simon-Assmann P, Bouziges F, Freund JN, Perrin-Schmitt F & Kedinger M (1990) Type IV collagen mRNA accumulates in the mesenchymal compartment at early stages of murine developing intestine. *J Cell Biol* **110**, 849–857.

22 Smola H, Stark HJ, Thiekötter G, Mirancea N, Krieg T & Fusenig NE (1998) Dynamics of basement membrane formation by keratinocyte-fibroblast interactions in organotypic skin culture. *Exp Cell Res* **239**, 399–410.

23 Cummings CF, Pedchenko V, Brown KL, Colon S, Rafi M, Jones-Paris C, Pokydeshava E, Liu M, Pastor-Pareja JC, Stothers C, Ero-Tolliver IA, McCall AS, Vanacore R, Bhave G, Santoro S, Blackwell TS, Zent R, Pozzi A & Hudson BG (2016) Extracellular chloride signals collagen IV network assembly during basement membrane formation. *J Cell Biol* **213**, 479–494.

24 Kühn K, Wiedemann H, Timpl R, Risteli J, Dieringer H, Voss T & Glanville RW (1981) Macromolecular structure of basement membrane collagens. *FEBS Lett* **125**, 123–128.

25 Aumailley M, Wiedemann H, Mann K & Timpl R (1989) Binding of nidogen and the laminin-nidogen complex to basement membrane collagen type IV. *Eur J Biochem* **184**, 241–248.

26 Yurchenco PD & Ruben GC (1987) Basement membrane structure in situ: Evidence for lateral associations in the type IV collagen network. *J Cell Biol* **105**, 2559–2568.

27 Mickel W, Münster S, Jawerth LM, Vader DA, Weitz DA, Sheppard AP, Mecke K, Fabry B & Schröder-Turk GE (2008) Robust pore size analysis of filamentous networks from three-dimensional confocal microscopy. *Biophys J* **95**, 6072–6080.

28 Yang YL, Leone LM & Kaufman LJ (2009) Elastic moduli of collagen gels can be predicted from two-dimensional confocal microscopy. *Biophys J* **97**, 2051–2060.

29 Wolf K, Alexander S, Schacht V, Coussens LM, von Andrian UH, van Rheenen J, Deryugina E & Friedl P (2009) Collagen-based cell migration models *in vitro* and *in vivo*. *Semin Cell Dev Biol* **20**,

931–941.

30 Despotović SZ, Milićević ĐN, Krmpot AJ, Pavlović AM, Živanović VD, Krivokapić Z, Pavlović VB, Lević S, Nikolić G & Rabasović MD (2020) Altered organization of collagen fibers in the uninvolved human colon mucosa 10 cm and 20 cm away from the malignant tumor. *Sci Rep* **10**, 6359.

31 Mathan M, Hermos JA & Trier JS (1972) Structural features of the epithelio-mesenchymal interface of rat duodenal mucosa during development. *J Cell Biol* **52**, 577–588.

32 Brown KL, Cummings CF, Vanacore RM & Hudson BG (2017) Building collagen IV smart scaffolds on the outside of cells. *Protein Sci* **26**, 2151–2161.

33 Smyth N, Vatansever HS, Murray P, Meyer M, Frie C, Paulsson M & Edgar D (1999) Absence of basement membranes after targeting the *LAMC1* gene results in embryonic lethality due to failure of endoderm differentiation. *J Cell Biol* **144**, 151–160.

34 Morin X, Daneman R, Zavortink M & Chia W (2001) A protein trap strategy to detect GFP-tagged proteins expressed from their endogenous loci in *Drosophila*. *Proc Natl Acad Sci U S A* **98**, 15050–15055.

35 Ihara S, Hagedorn EJ, Morrissey M a, Chi Q, Motegi F, Kramer JM & Sherwood DR (2011) Basement membrane sliding and targeted adhesion remodels tissue boundaries during uterine-vulval attachment in *Caenorhabditis elegans*. *Nat Cell Biol* **13**, 641–651.

36 Ramanujan S, Pluen A, McKee TD, Brown EB, Boucher Y & Jain RK (2002) Diffusion and convection in collagen gels: Implications for transport in the tumor interstitium. *Biophys J* **83**, 1650–1660.

37 Furuyama A & Mochitate K (2000) Assembly of the exogenous extracellular matrix during basement membrane formation by alveolar epithelial cells *in vitro*. *J Cell Sci* **113**, 859–868.

38 Sanz-Moreno V, Gadea G, Ahn J, Paterson H, Marra P, Pinner S, Sahai E & Marshall CJ (2008) Rac activation and inactivation control plasticity of tumor cell movement. *Cell* **135**, 510–523.

39 Yamazaki D, Kurisu S & Takenawa T (2009) Involvement of Rac and Rho signaling in cancer cell motility in 3D substrates. *Oncogene* **28**, 1570–1583.

40 Fukumoto M, Kurisu S, Yamada T & Takenawa T (2015) α-actinin-4 enhances colorectal cancer cell invasion by suppressing focal adhesion maturation. *PLoS One* **10**, e0120616.

41 Fraley SI, Feng Y, Krishnamurthy R, Kim DH, Celedon A, Longmore GD & Wirtz D (2010) A distinctive role for focal adhesion proteins in three-dimensional cell motility. *Nat Cell Biol* **12**, 598–604.

42 Yurchenco PD, Tsilibary EC, Charonis AS & Furthmayr H (1986) Models for the self-assembly of basement membrane. *J Histochem Cytochem* **34**, 93–102.

43 Patel TR, Bernards C, Meier M, McEleney K, Winzor DJ, Koch M & Stetefeld J (2014) Structural elucidation of full-length nidogen and the laminin-nidogen complex in solution. *Matrix Biol* **33**, 60–

67.

44 Shin JH, Gardelt ML, Mahadevan L, Matsudaira P & Weitz DA (2004) Relating microstructure to rheology of a bundled and cross-linked F-actin network *in vitro*. *Proc Natl Acad Sci U S A* **101**, 9636–9641.

45 Granger DN, Mortillaro NA, Kvietys PR, Rutili G, Parker JC & Taylor AE (1980) Role of the interstitial matrix during intestinal volume absorption. *Am J Physiol - Gastrointest Liver Physiol* **238**, G183-G189.

46 Duncan KG, Fessler LI, Bachinger HP & Fessler JH (1983) Procollagen IV. Association to tetramers. *J Biol Chem* **258**, 5869–5877.

47 Engelholm LH, List K, Netzel-Arnett S, Cukierman E, Mitola DJ, Aaronson H, Kjøller L, Larsen JK, Yamada KM, Strickland DK, Holmbeck K, Danø K, Birkedal-Hansen H, Behrendt N & Bugge TH (2003) uPARAP/Endo180 is essential for cellular uptake of collagen and promotes fibroblast collagen adhesion. *J Cell Biol* **160**, 1009–1015.

48 Langholz O, Röckel D, Mauch C, Kozlowska E, Bank I, Krieg T & Eckes B (1995) Collagen and collagenase gene expression in three-dimensional collagen lattices are differentially regulated by α1β1 and α2β1 integrins. *J Cell Biol* **131**, 1903–1915.

49 Gardner H, Kreidberg J, Koteliansky V & Jaenisch R (1996) Deletion of integrin α1 by homologous recombination permits normal murine development but gives rise to a specific deficit in cell adhesion. *Dev Biol* **175**, 301–313.

50 Jayadev R, Chi Q, Keeley DP, Hastie EL, Kelley LC & Sherwood DR (2019) α-Integrins dictate distinct modes of type IV collagen recruitment to basement membranes. *J Cell Biol* **218**, 3098–3116.

51 Sardone F, Santi S, Tagliavini F, Traina F, Merlini L, Squarzoni S, Cescon M, Wagener R, Maraldi NM, Bonaldo P, Faldini C & Sabatelli P (2016) Collagen VI–NG2 axis in human tendon fibroblasts under conditions mimicking injury response. *Matrix Biol* **55**, 90–105.

52 Canty EG, Lu Y, Meadows RS, Shaw MK, Holmes DF & Kadler KE (2004) Coalignment of plasma membrane channels and protrusions (fibropositors) specifies the parallelism of tendon. *J Cell Biol* **165**, 553–563.

53 Matsubayashi Y, Louani A, Dragu A, Sánchez-Sánchez BJ, Serna-Morales E, Yolland L, Gyoergy A, Vizcay G, Fleck RA, Heddleston JM, Chew T-L, Siekhaus DE & Stramer BM (2017) A moving source of matrix components is essential for *de novo* basement membrane formation. *Curr Biol* **27**, 3526-3534.e4.

54 Pastor-Pareja JC & Xu T (2011) Shaping cells and organs in *Drosophila* by opposing roles of fat body-secreted collagen IV and perlecan. *Dev Cell* **21**, 245–256.

55 Graham PL, Johnson JJ, Wang S, Sibley MH, Gupta MC & Kramer JM (1997) Type IV collagen is detectable in most, but not all, basement membranes of *Caenorhabditis elegans* and assembles on

tissues that do not express it. *J Cell Biol* **137**, 1171–1183.

56 Barker TH, Framson P, Puolakkainen PA, Reed M, Funk SE & Sage EH (2005) Matricellular homologs in the foreign body response: Hevin suppresses inflammation, but hevin and SPARC together diminish angiogenesis. *Am J Pathol* **166**, 923–933.

57 Wang H, Lacoche S, Huang L, Xue B & Muthuswamy SK (2013) Rotational motion during three-dimensional morphogenesis of mammary epithelial acini relates to laminin matrix assembly. *Proc Natl Acad Sci U S A* **110**, 163–168.

58 Haigo SL & Bilder D (2011) Global tissue revolutions in a morphogenetic movement controlling elongation. *Science* **331**, 1071–1074.

59 Mifflin RC, Pinchuk I V., Saada JI & Powell DW (2011) Intestinal myofibroblasts: Targets for stem cell therapy. *Am J Physiol - Gastrointest Liver Physiol* **300**, 684–696.

60 Endale M, Ahlfeld S, Bao E, Chen X, Green J, Bess Z, Weirauch MT, Xu Y & Perl AK (2017) Temporal, spatial, and phenotypical changes of PDGFRα expressing fibroblasts during late lung development. *Dev Biol* **425**, 161–175.

61 Kaissling B & Le Hir M (2008) The renal cortical interstitium: Morphological and functional aspects. *Histochem Cell Biol* **130**, 247–262.

62 Tsutsui K, Machida H, Nakagawa A, Ahn K, Morita R, Sekiguchi K, Miner JH & Fujiwara H (2021) Mapping the molecular and structural specialization of the skin basement membrane for inter-tissue interactions. *Nat Commun* **12**, 2577.

63 Joyce NC, Haire MF & Palade GE (1987) Morphologic and biochemical evidence for a contractile cell network within the rat intestinal mucosa. *Gastroenterology* **92**, 68–81.

64 Sato H, Naito I, Momota R, Naomoto Y, Yamatsuji T, Sado Y, Ninomiya Y & Ohtsuka A (2007) The differential distribution of type IV collagen α chains in the subepithelial basement membrane of the human alimentary canal. *Arch Histol Cytol* **70**, 313–323.

Table 1. Gene-specific primers and cycle numbers used for RT-PCR

Target		Primer sequence (5'-3')	Size of PCR products	Cycle number
COL4A1	F	gagcccatgcccatgtcaat	323 bp	30
	R	gcgagccaaaagctgtaagcgtt		
COL4A2	F	gcatcggctacctcctggtgaa	597 bp	30
	R	cctggaagctctgctcgggaat		
COL4A3	F	gcagagcccttgagccttat	254 bp	35
	R	gcacgttcctcttccatgaca		
COL4A4	F	ctggactgggtatagtctgttat	357 bp	35
	R	cctgtgtgcatcaggaatgaata		
COL4A5	F	ccatgcctttcatgttctgcaa	394 bp	30
	R	ctgtaggagttggcatagtagt		
COL4A6	F	gagtgggctacacgttggta	250 bp	35
	R	gtagtggagagccagtaagatt		
LAMA5	F	ctggagtacaacgaggtcaa	251 bp	30
	R	gagtactcggtggtgcagat		
LAMC1	F	gagcggttgattgaaatcgca	230 bp	30
	R	gtcctcagaagcaggttgta		
NID1	F	cattgggagagctagtctaca	247 bp	30
	R	ccagtctgtccagtaaaggtt		
NID2	F	ggatgagagagagaccagaa	278 bp	30
	R	tgaagacctcggtgttggaa		
Perlecan	F	ctgtgtcgagatggattcaaa	246 bp	30
	R	gaagccatcatcgtggaaata		
CFL1	F	ggaggtgaagaagcgcaaga	420 bp	25

	R	cacaaaggcttgccctcca		
WASF2	F	gcagcctgagtaaatatgca	450 bp	25
	R	cattccctcgatttggatta		
NCKAP1	F	tgtaccaaacatggtggtat	154 bp	25
	R	acttgttagaagttctgaag		
ACTN1	F	gtccatcggagccgaagaaa	355 bp	25
	R	gtcttcggcatccagcatct		

Legends to figures

Figure 1.

The BM-like structure was formed by co-culture of DLD-1 and 36T-2 cells using collagen I gel. (A) Schematic representation of co-culture of DLD-1 and 36T-2 cells using collagen I gel. (B) Epifluorescence micrographs of the basal regions of DLD-1 cells co-cultured with 36T-2 cells for the indicated days. Gels were immunostained for collagen IV (top) and laminin (middle), and cell nuclei were stained with DAPI (bottom). (C) Epifluorescence micrographs of the basal regions of DLD-1 cells of a 4-day co-culture gel. Gels were immunostained for collagen IV (green), laminin (magenta) and Scrib (gray) with (left two panels) or without (right two panels) permeabilization by 0.2% Triton-X100/G-PBS for 10 min. Note that laminin and collagen IV were stained similarly in both conditions while antibodies against Scrib, a basolateral membrane marker, stained only the permeabilized sample. (D) Confocal micrographs of a 4-day co-culture gel immunostained for collagen IV (green) and laminin (magenta). Actin cytoskeleton and cell nuclei were fluorescently labelled with phalloidin (red) and DAPI (cyan). Maximum projections of 8 confocal slices (~1.2 μm thickness) are shown, accompanying respective vertical section images below. Right panels show magnified images of the boxed area. The white arrows indicate direction from apical to basal. (E) Epifluorescence micrographs of the basal regions of DLD-1 cells of a 4-day co-culture gel. Gels were immunostained for perlecan, nidogen-1 and laminin. The rightmost panel shows the merged image. (F) Epifluorescence micrographs of the basal regions of DLD-1 cells cultured on collagen I gel without 36T-2 cells for 4 days. Gels were immunostained for collagen IV and laminin (left column) or nidogen-1 and perlecan (right column). Bars, 40 μm (B and F) and 20 μm (C, D and E). Each micrograph is representative of two (C, E and F) or three (B and D) independent experiments that produced similar results.

Figure 2.

Semi-quantitative RT-PCR analysis of expression levels of BM components. 36T-2 or DLD-1 cells were cultured separately on plastic dishes, from which respective total RNAs were isolated (lane 1,2). Total RNAs of the co-culture condition were isolated from the 4-day co-culture gels containing both DLD-1 and 36T-2 cells (lane 3). Total RNAs of MCF10A human mammary epithelial cells were used as positive control (lane 4). The amount of cDNA templates used for analysis was doubled in the co-culture condition compared to other conditions. Primer pairs used for analysis are listed in Table 1. *CFL1* expression was used as an internal control. Two independent experiments gave similar results.

Figure 3.

Collagen IV in the BM-like structure is derived from 36T-2 cells. (A) RT-PCR analysis of *COL4A1* and *COL4A2* expression in 36T-2 cells (top and middle) or *COL4A1* expression in DLD-1 cells

(bottom). Cells were treated with the indicated siRNAs. *CFL1* expression was used as an internal control. (B) Epifluorescence micrographs of the basal regions of DLD-1 cells co-cultured for 4 days. Three columns from the left show non-treated DLD-1 cells co-cultured with 36T-2 cells treated with the indicated siRNAs. Two columns from the right show DLD-1 cells treated with the indicated siRNAs co-cultured with non-treated 36T-2 cells. Gels were immunostained as in Fig. 1B. The bottom row indicates high magnification images of the boxed areas. (C) Quantification of immunofluorescence intensities. All data in the graph represent means ±SE values of three independent experiments. Significance was determined using unpaired two-sided Student's *t*-test. **, $p < 0.01$; n.s., not significant. (D and E) Epifluorescence micrographs of the basal regions of non-treated DLD-1 cells co-cultured with 36T-2 cells treated with the indicated siRNAs. Gels were immunostained for nidogen-1 and perlecan. The insets show magnified images of the boxed areas. Bars, 40 μm. Each micrograph is representative of three independent experiments.

Figure 4.

Laminin deposition at the base of DLD-1 cells is a pre-requisite for the recruitment of other BM components. (A) RT-PCR analysis of *LAMC1* expression in 36T-2 cells (upper) or DLD-1 cells (lower). Cells were treated with the indicated siRNAs. *CFL1* expression was used as an internal control. (B) Epifluorescence micrographs of the basal regions of DLD-1 cells co-cultured for 4 days. Both DLD-1 cells and 36T-2 cells were treated with siControl (left column) or siLAMC1 (right column), prior to the start of co-culture. Gels were immunostained for collagen IV (green) and laminin (magenta), and cell nuclei were stained with DAPI. (C) Nidogen-1 and cell nuclei were stained and shown as in (B). (D) Quantification of immunofluorescence intensities. All data in the graph represent means ±SE values of three independent experiments. Significance was determined using unpaired two-sided Student's *t*-test. **, $p < 0.01$; *, $p < 0.05$. Bars, 40 μm. Each micrograph is representative of three independent experiments.

Figure 5.

Construction of EGFP-tagged human COL4A1 to visualize collagen IV derived from a single 36T-2 cell. (A) Domain structure of collagen IV α1 chain and candidate constructs of EGFP-inserted COL4A1. COL4A1 consists of 7S domain at the N-terminus, the glycine-X-Y (GXY) repeat sequence that forms collagenous triple helix, and the globular non-collagenous 1 (NC1) domain at the C-terminus. We inserted EGFP just after the amino acid of COL4A1 indicated on the left or at the C-terminus. SS, signal peptide sequence; Cter, C-terminus. (B) Epifluorescence and phase contrast micrographs of 36T-2 cells transiently transfected with the indicated COL4A1 constructs. Thirty-six hours after transfection, 36T-2 cells were immunostained for EGFP (green) and endogenous COL4A2

(magenta). The construct 32Ala was colocalized with endogenous COL4A2 both inside and outside of the cell. 641Ile was not colocalized with COL4A2 and accumulated intracellularly. 940Lys was detected outside of the cell but not colocalized with COL4A2. EGFP insertion at C-terminus was well colocalized with COL4A2 like 32Ala. (C) Epifluorescence micrographs of the basal regions of DLD-1 cells co-cultured for 4 days on a collagen gel containing 36T-2 cells stably expressing EGFP-COL4A1 (32Ala). Gels were immunostained for EGFP (green) and collagen IV (magenta). (D) Epifluorescence micrographs of EGFP-COL4A1 distribution in the basal regions of DLD-1 cells co-cultured for 4 days with 36T-2 cell mixtures including wild-type and EGFP-COL4A1-expressing cells. Gels were immunostained for EGFP (green) and collagen IV (magenta). The arrowheads indicate deposited EGFP-COL4A1. The brackets indicate the cell body of an EGFP-COL4A1-expressing 36T-2 cell, respectively. Bars, 20 μm (B) and 40 μm (C and D). Each micrograph is representative of two (B) or three (C and D) independent experiments that produced similar results.

Figure 6.

36T-2 cells deposit collagen IV in proximity to DLD-1 epithelial cells. (A) Schematic representation of collagen I gel overlay (OL) co-culture. (B) Confocal micrographs of the basal region of DLD-1 cells co-cultured with 36T-2 cells for 4 days. Left, middle, and right columns show conditions without OL, with 2.1 mg/mL collagen I gel OL, and with 1.3 mg/mL OL, respectively. Gels were immunostained for collagen IV (green), laminin (red) and nidogen-1(blue), and cell nuclei were stained with DAPI. Merged images are shown at the bottom row. Bar, 40 μm. Each micrograph is representative of six (w/o OL), seven (with 2.1 mg/mL OL) or four (with 1.3 mg/mL OL) independent experiments. (C) Quantification of immunofluorescence intensities. All data in the graph represent means ±SE values of six (w/o OL), seven (with 2.1 mg/mL OL) or four (with 1.3 mg/mL OL) independent experiments. Significance was determined using unpaired two-sided Student's *t*-test. **, $p < 0.01$; *, $p < 0.05$; n.s., not significant. (D) Western blotting (WB) of the culture medium taken from co-cultures without OL or with 2.1 mg/mL collagen I OL. Coomassie brilliant blue (CBB) staining shows a loading control. The blot is representative of two independent experiments with similar results.

Figure 7.

BM Collagen IV deposition is promoted by direct contact between DLD-1 cells and 36T-2 cells. (A) Epifluorescence micrographs of the basal regions of DLD-1 cells co-cultured with 36T-2 cells using Transwell chambers. Co-culture topologies are illustrated at the top of each column. Transwell membranes including cells were immunostained for collagen IV (green) and laminin (magenta). For the condition (iii), F-actin was simultaneously visualized by phalloidin to identify 36T-2 fibroblasts. In addition, triple immunostaining with collagen IV (green), laminin (red) and nidogen-1 (blue) was

performed for the condition (iii) and is shown at the right column. The boxed area is enlarged and the image is shown as zoom. Fibrous collagen IV deposition is denoted by arrowheads. 36T-2 cell bodies are indicated by brackets. Bar, 40 μm. Each micrograph is representative of three independent experiments that produced similar results. (B) Western blotting of the culture medium taken from the lower well of Transwell co-cultures. Each condition corresponds to the illustrations in A. As a negative control, Transwell culture of DLD-1 without fibroblasts was performed and the sample was indicated by (-). CBB was used as a loading control. The blot is representative of two independent experiments with similar results.

Figure 8.

Collagen IV is deposited by 36T-2 cells as aggregates and rearranged into fibril-like structures in proximity to DLD-1 cells (A) A time-lapse series from live cell imaging of the co-culture of EGFP-COL4A1-expressing 36T-2 cells and histone H2B-mCherry-expressing DLD-1 cells. EGFP-COL4A1 and histone H2B-mCherry are colored in green and magenta, respectively. Note that collagen IV aggregates (denoted by arrowheads) were left behind the migrating fibroblasts (denoted by asterisks). Time is shown as hour:minute. Images were taken from the boxed region of Movie S1. (B) Collagen IV aggregates transformed into fibrils via presumptive traction force exerted by 36T-2 cells (denoted by asterisks). Rearranging collagen IV is denoted by brackets. See Movie S2. (C) Collagen IV aggregates (denoted by arrowheads) that were not adhered to DLD-1 cells were retrieved by fibroblasts. Aggregate-depositing fibroblasts (*) and aggregate-retrieving fibroblasts (+) were denoted, respectively. See Movie S3. Bar, 20 μm.

Figure 9.

36T-2 cell motility promotes collagen IV deposition at the BM region. (A) RT-PCR analysis of *WAVE2*, *NCKAP1*, and *ACTN1* expression levels in 36T-2 cells treated with the indicated siRNAs. *CFL1* expression was used as an internal control. (B) Epifluorescence micrographs of the basal regions of DLD-1 cells co-cultured with 36T-2 cells treated with the indicated siRNAs. Gels were immunostained as in Fig. 1B. Bar, 40 μm. Each micrograph is representative of three independent experiments. (C) Quantification of immunofluorescence intensities of images shown in (B). All data in the graph represent means ±SE values of three independent experiments. Significance was determined using unpaired two-sided Student's *t*-test. *, $p < 0.05$. (D) Western blotting of the culture media collected from the indicated culture conditions. The blot is representative of three independent experiments with similar results.

Supporting Information

Movie S1.

The full movie of Fig. 8A.

Movie S2.

The full movie of Fig. 8B.

Movie S3.

The full movie of Fig. 8C.

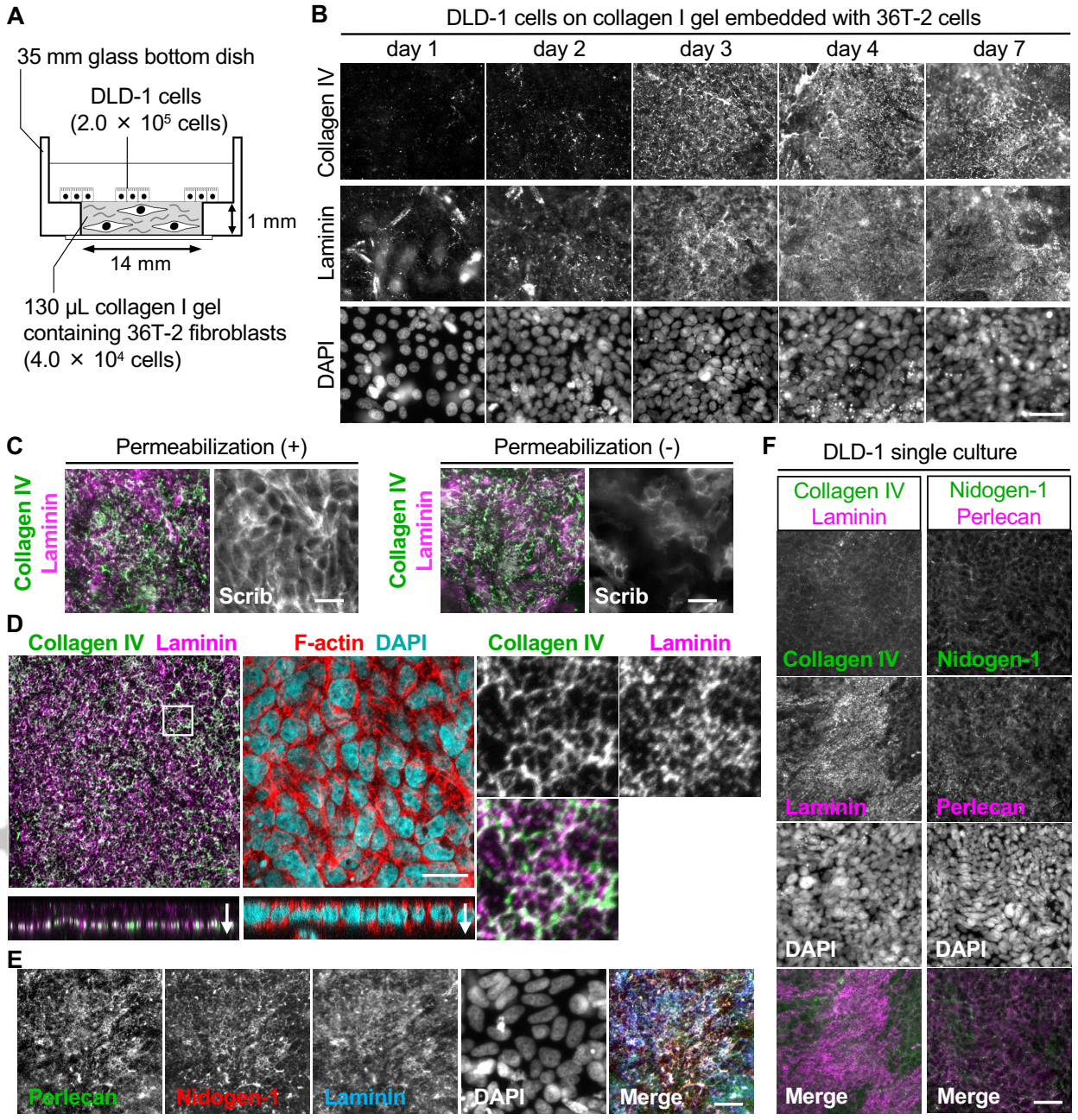
A
35 mm glass bottom dish
DLD-1 cells
(2.0 × 10^5 cells)
1 mm
14 mm
130 µL collagen I gel
containing 36T-2 fibroblasts
(4.0 × 10^4 cells)
B
DLD-1 cells on collagen I gel embedded with 36T-2 cells
day 1
day 2
day 3
day 4
day 7
Collagen IV
Laminin
DAPI
C
Permeabilization (+)
Permeabilization (-)
Collagen IV
Laminin
Scrib
D
Collagen IV
Laminin
F-actin
DAPI
E
Perlecan
Nidogen-1
Laminin
DAPI
Merge
F
DLD-1 single culture
Collagen IV
Laminin
Nidogen-1
Perlecan
DAPI
Merge

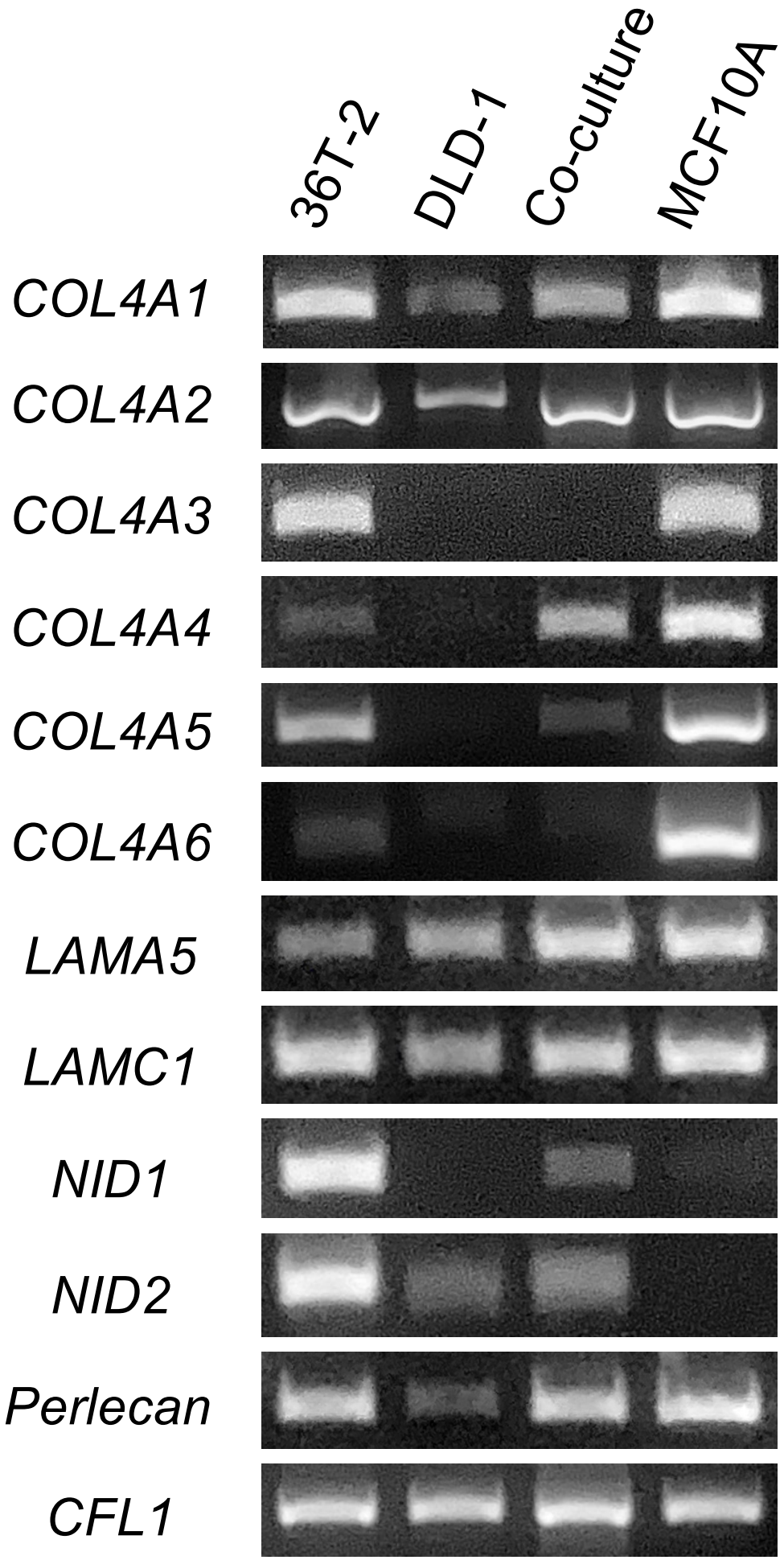
36T-2
DLD-1
Co-culture
MCF10A
COL4A1
COL4A2
COL4A3
COL4A4
COL4A5
COL4A6
LAMA5
LAMC1
NID1
NID2
Perlecan
CFL1

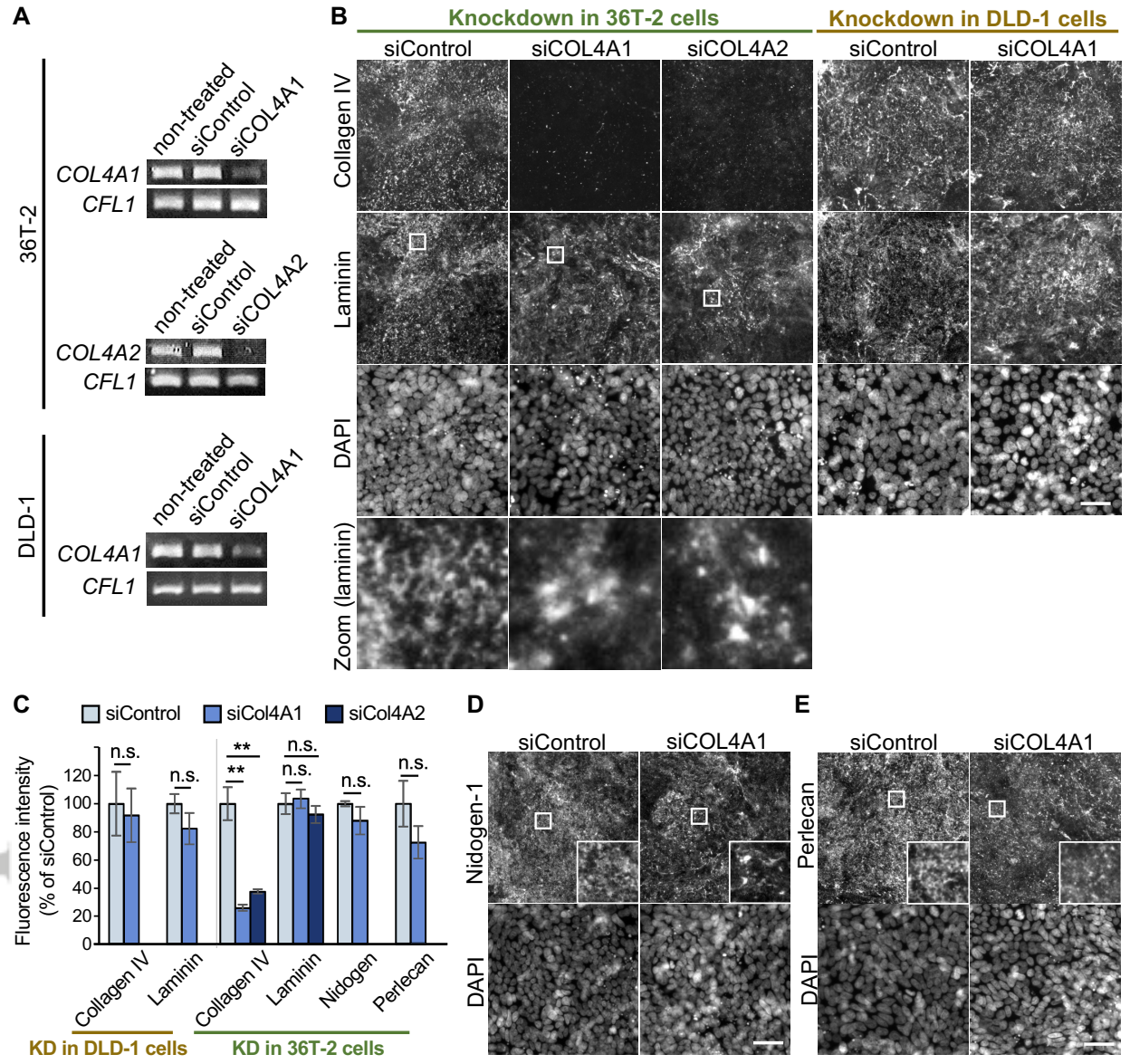
A
36T-2
non-treated
siControl
siCOL4A1
COL4A1
CFL1
non-treated
siControl
siCOL4A2
COL4A2
CFL1
DLD-1
non-treated
siControl
siCOL4A1
COL4A1
CFL1
B
Knockdown in 36T-2 cells
Knockdown in DLD-1 cells
siControl
siCOL4A1
siCOL4A2
siControl
siCOL4A1
Collagen IV
Laminin
DAPI
Zoom (laminin)
C
siControl
siCol4A1
siCol4A2
Fluorescence intensity (% of siControl)
120
100
80
60
40
20
0
n.s.
n.s.
**
**
n.s.
n.s.
n.s.
n.s.
Collagen IV
Laminin
Collagen IV
Laminin
Nidogen
Perlecan
KD in DLD-1 cells
KD in 36T-2 cells
D
siControl
siCOL4A1
Nidogen-1
DAPI
E
siControl
siCOL4A1
Perlecan
DAPI

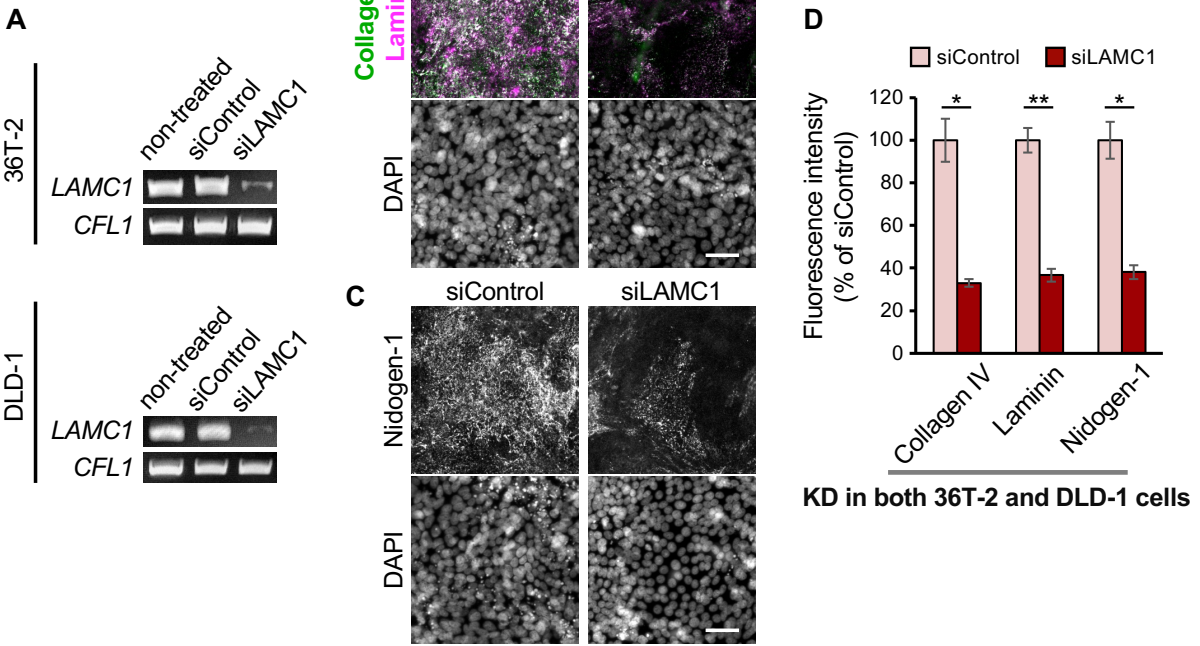
A
36T-2
non-treated
siControl
siLAMC1
LAMC1
CFL1
DLD-1
non-treated
siControl
siLAMC1
LAMC1
CFL1
B
siControl
siLAMC1
Collagen IV
Laminin
DAPI
C
siControl
siLAMC1
Nidogen-1
DAPI
D
siControl
siLAMC1
Fluorescence intensity
(% of siControl)
120
100
80
60
40
20
0
*
**
*
Collagen IV
Laminin
Nidogen-1
KD in both 36T-2 and DLD-1 cells

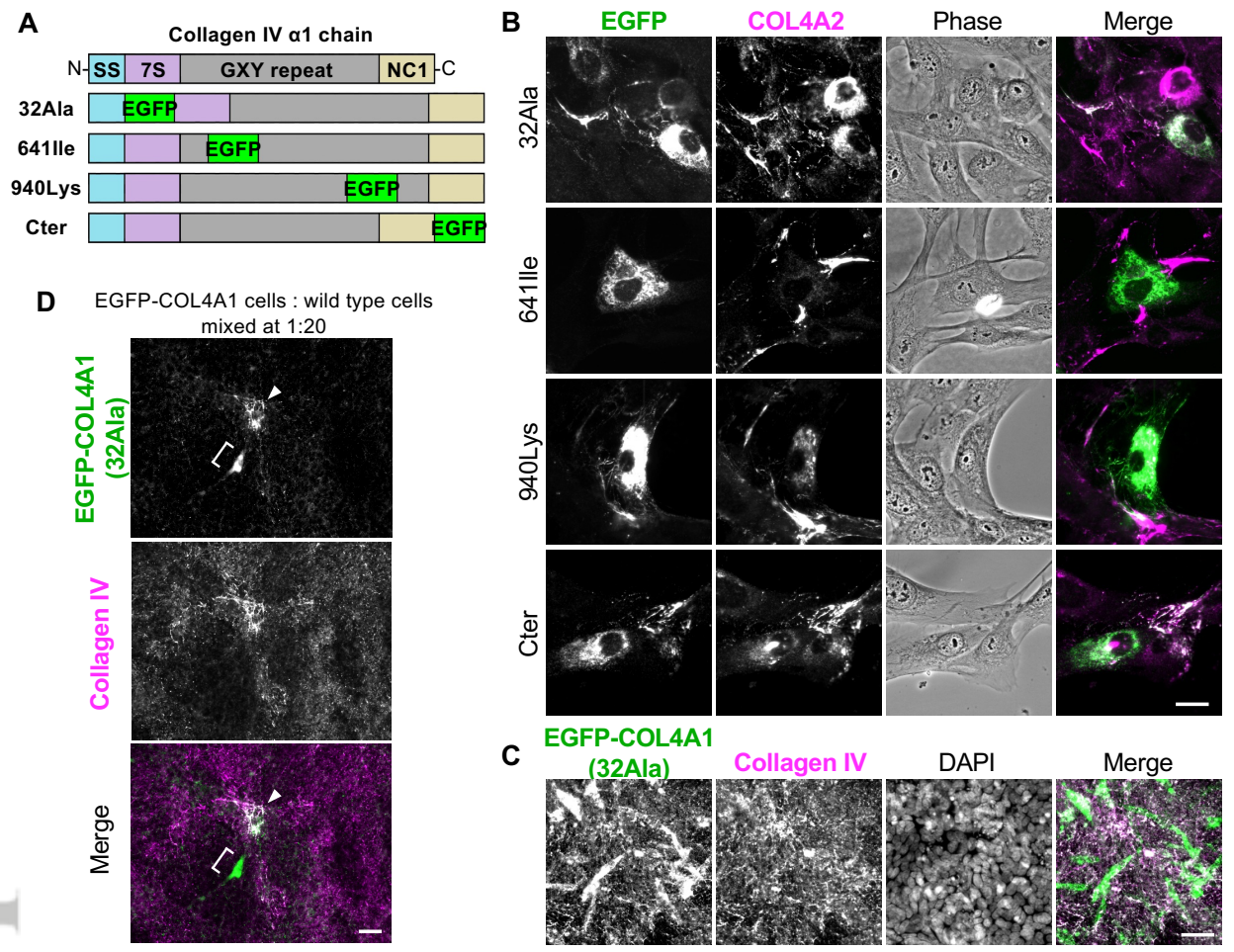
A
Collagen IV α1 chain
N-
SS
7S
GXY repeat
NC1
-C
32Ala
EGFP
641Ile
EGFP
940Lys
EGFP
Cter
EGFP
B
EGFP
COL4A2
Phase
Merge
32Ala
641Ile
940Lys
Cter
C
EGFP-COL4A1 (32Ala)
Collagen IV
DAPI
Merge
D
EGFP-COL4A1 cells : wild type cells mixed at 1:20
EGFP-COL4A1 (32Ala)
Collagen IV
Merge

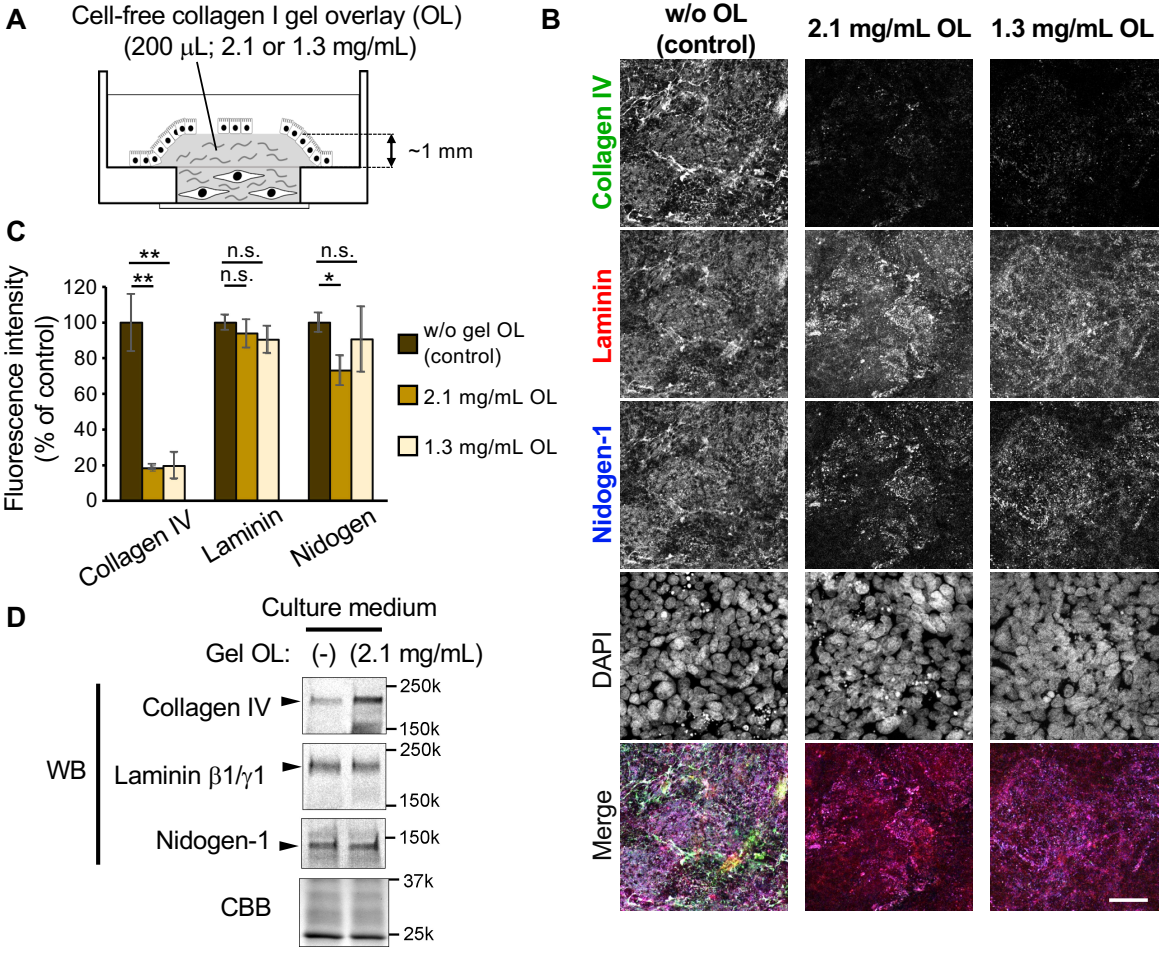
A
Cell-free collagen I gel overlay (OL)
(200 μL; 2.1 or 1.3 mg/mL)
~1 mm
B
w/o OL (control)
2.1 mg/mL OL
1.3 mg/mL OL
Collagen IV
Laminin
Nidogen-1
DAPI
Merge
C
Fluorescence intensity (% of control)
120
100
80
60
40
20
0
**
**
n.s.
n.s.
n.s.
*
w/o gel OL (control)
2.1 mg/mL OL
1.3 mg/mL OL
Collagen IV
Laminin
Nidogen
D
Culture medium
Gel OL: (-) (2.1 mg/mL)
WB
Collagen IV
Laminin β1/γ1
Nidogen-1
CBB
250k
150k
250k
150k
150k
37k
25k

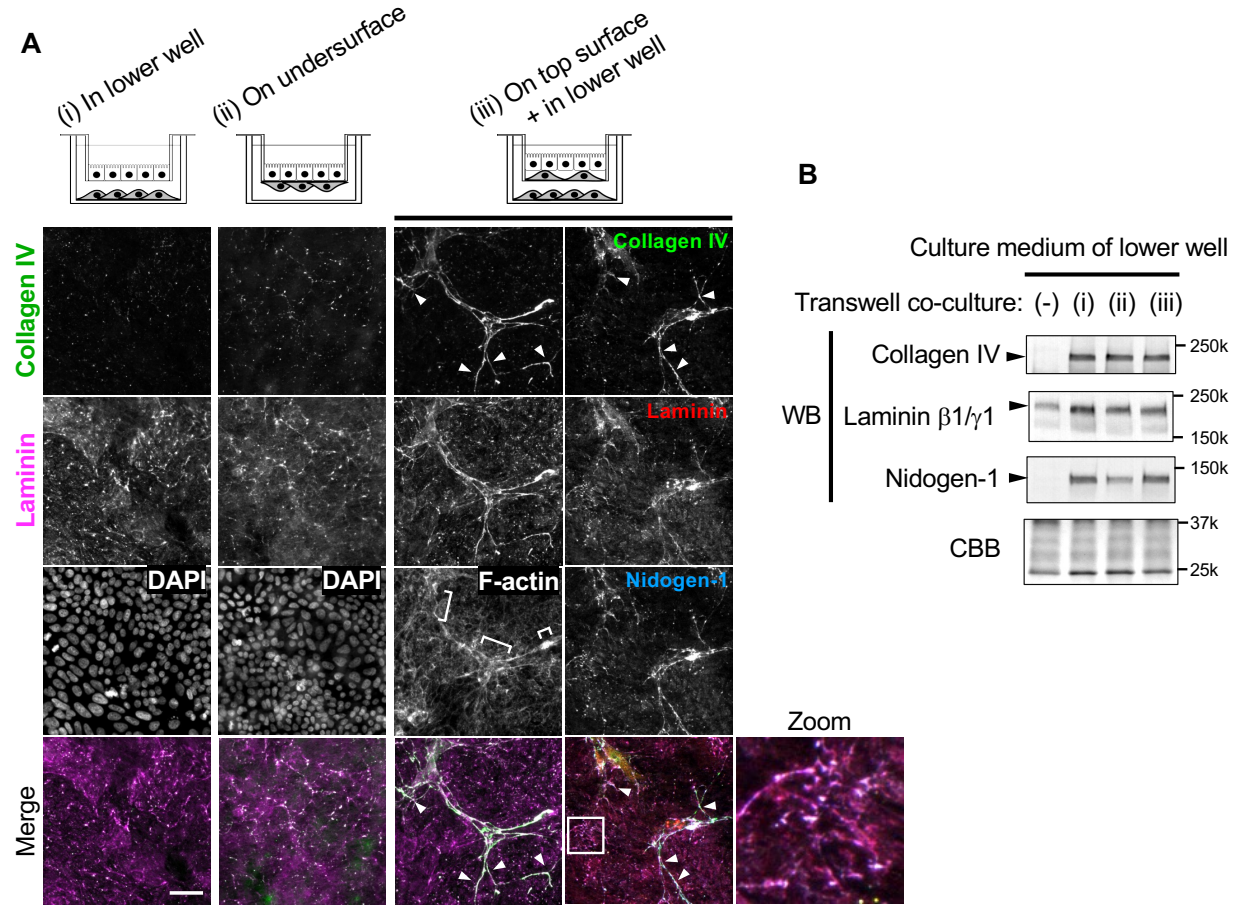
A
(i) In lower well
(ii) On undersurface
(iii) On top surface + in lower well
Collagen IV
Laminin
DAPI
DAPI
F-actin
Nidogen-1
Merge
Zoom
B
Culture medium of lower well
Transwell co-culture: (-) (i) (ii) (iii)
WB
Collagen IV
Laminin β1/γ1
Nidogen-1
CBB
250k
250k
150k
150k
37k
25k

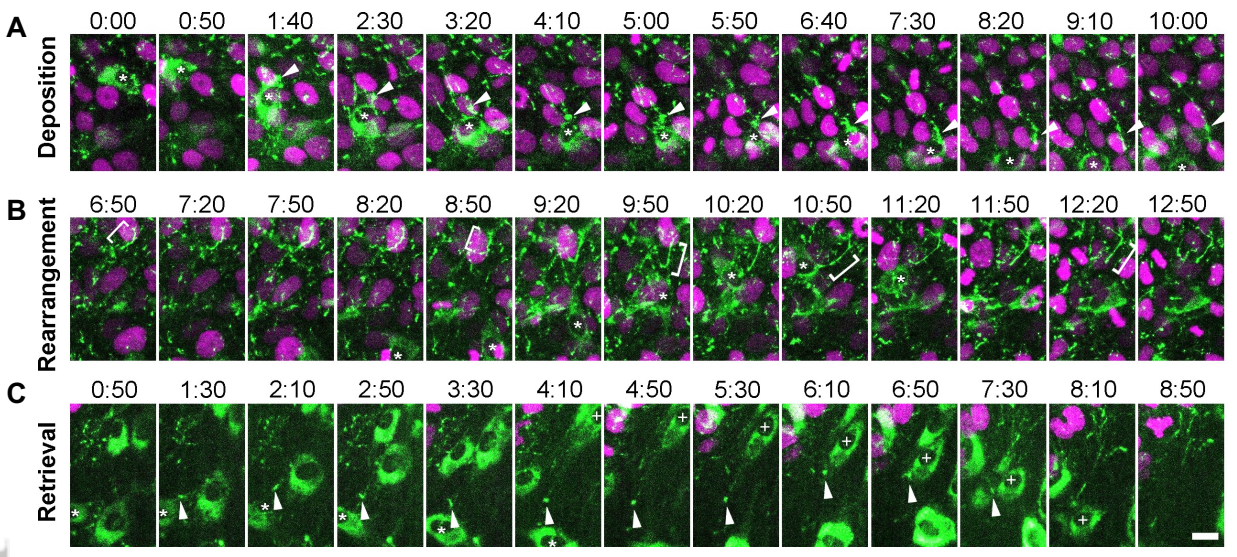
A
Deposition
0:00
0:50
1:40
2:30
3:20
4:10
5:00
5:50
6:40
7:30
8:20
9:10
10:00
B
Rearrangement
6:50
7:20
7:50
8:20
8:50
9:20
9:50
10:20
10:50
11:20
11:50
12:20
12:50
C
Retrieval
0:50
1:30
2:10
2:50
3:30
4:10
4:50
5:30
6:10
6:50
7:30
8:10
8:50

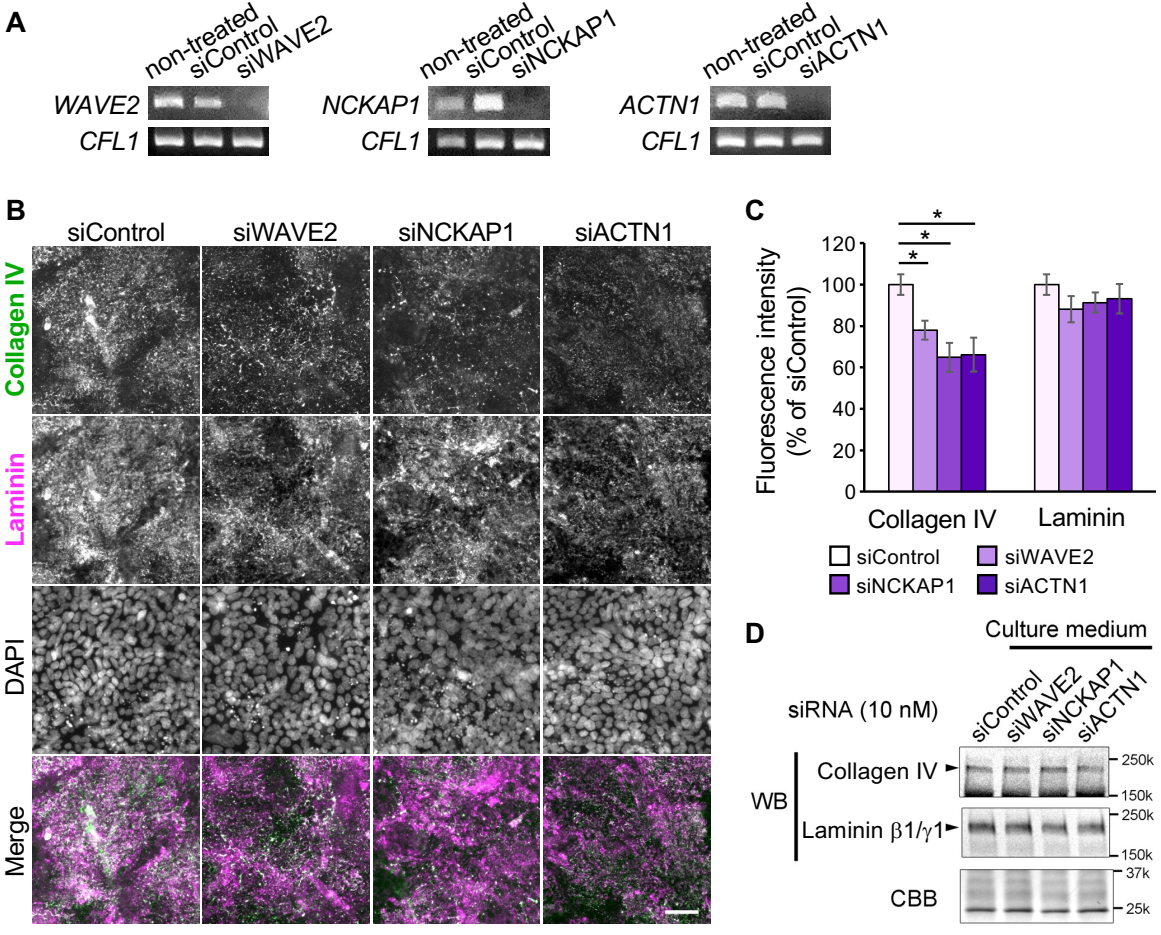
A
non-treated
siControl
siWAVE2
WAVE2
CFL1
non-treated
siControl
siNCKAP1
NCKAP1
CFL1
non-treated
siControl
siACTN1
ACTN1
CFL1
B
siControl
siWAVE2
siNCKAP1
siACTN1
Collagen IV
Laminin
DAPI
Merge
C
Fluorescence intensity
(% of siControl)
120
100
80
60
40
20
0
*
*
*
Collagen IV
Laminin
siControl
siWAVE2
siNCKAP1
siACTN1
D
Culture medium
siRNA (10 nM)
siControl
siWAVE2
siNCKAP1
siACTN1
WB
Collagen IV
Laminin β1/γ1
250k
150k
250k
150k
CBB
37k
25k